AAC Accepted Manuscript Posted Online 1 June 2020
Antimicrob. Agents Chemother. doi:10.1128/AAC.00289-20

Identification of estrogen receptor modulators as inhibitors of flavivirus infection

Nicholas S. Eyre [a,b,*], Emily N. Kirby [a,b,1], Daniel R. Anfiteatro [a,b,1], Gustavo Bracho [c,1], Alice G. Russo [d], Peter A. White [d], Amanda L. Aloia [c,2], Michael R. Beard [a,b,2]

[a] Research Centre for Infectious Diseases, School of Biological Sciences, University of Adelaide, Adelaide, Australia

[b] Centre for Cancer Biology, SA Pathology, Adelaide, Australia

[c] Cell Screen SA, Flinders Centre for Innovation in Cancer, Flinders University, Bedford Park, Australia.

[d] School of Biotechnology and Biomolecular Sciences, Faculty of Science, The University of New South Wales, Sydney, Australia.

[*] Address correspondence to: nicholas.eyre@adelaide.edu.au (N.S.E.)

[1] E.N.K., D.R.A. and G.B. contributed equally to this work. Author order was determined randomly.

[2] A.L.A. and M.R.B. contributed equally to this work. Author order was determined in order of increasing seniority.

Keywords: flavivirus, dengue virus, Zika virus, West Nile virus, high-throughput screening, antiviral, estrogen receptor.

Running Title: Inhibition of flavivirus infections by synthetic estrogens.

Abstract Word Count: 186 words. Main Text Word Count (excluding Acknowledgements, References and Figure Legends): 7095 words.

ABSTRACT

Flaviviruses such as Zika virus (ZIKV), dengue virus (DENV) and West Nile virus (WNV) are major global pathogens for which safe and effective antiviral therapies are not currently available. To identify antiviral small molecules with well-characterized safety and bioavailability profiles we screened a library of 2,907 approved drugs and pharmacologically active compounds for inhibitors of ZIKV infection using a high-throughput cell-based immunofluorescence assay. Interestingly, estrogen receptor modulators raloxifene hydrochloride and quinestrol were amongst 15 compounds that significantly inhibited ZIKV infection in repeat screens. Subsequent validation studies revealed that these drugs effectively inhibit ZIKV, DENV and WNV (Kunjin strain) infection at low micromolar concentrations with minimal cytotoxicity in Huh-7.5 hepatoma cells and HTR-8 placental trophoblast cells. Since these cells lack detectable expression of estrogen receptors-α and -β (ER-α and ER-β) and similar antiviral effects were observed in the context of subgenomic DENV and ZIKV replicons, these compounds appear to inhibit viral RNA replication in a manner that is independent of their known effects on estrogen receptor signaling. Taken together, quinestrol, raloxifene hydrochloride and structurally related analogues warrant further investigation as potential therapeutics for treatment of flavivirus infections.

INTRODUCTION

Mosquito-borne flaviviruses such as Zika virus (ZIKV), dengue virus (DENV) and West Nile virus (WNV) are responsible for significant morbidity and mortality worldwide. For example, DENV, which is classified into four antigenically distinct serotypes (DENV1-4), is estimated to cause ~100 million symptomatic infections and ~25,000 deaths each year (1). In contrast, closely related ZIKV was thought to only cause mild febrile illness until recent large outbreaks in 2007 in the Pacific islands, in 2013 in French Polynesia and in 2014-2016 in South America revealed the unexpected association of ZIKV with serious neurodevelopmental disorders in infants and Guillain-Barré syndrome in infected adults (2). Interestingly, while ZIKV is predominantly transmitted via mosquitoes, recent studies involving clinical samples and animal models have shown that it can also spread vertically from the pregnant mother to developing foetus and via sexual contact (3). In the developing foetus ZIKV targets neural progenitor cells and limits their growth and induces apoptosis, providing a likely mechanism for ZIKV-induced congenital microcephaly and other neurodevelopmental disorders that are now collectively referred to as Zika congenital syndrome (ZCS) (2, 4-8).

The recent explosive outbreak of ZIKV and continual seasonal outbreaks of DENV and other related flaviviruses highlight the need for safe and effective preventative vaccines and therapeutic treatments to combat the spread and impact of these flaviviruses. While a vaccine for DENV is now available, due to its moderate efficacy and safety concerns related to sensitization of unexposed individuals to more severe disease, there remains an urgent need for improved vaccines that are ideally effective against multiple DENV serotypes and related flaviviruses, but do not exacerbate viral infection and disease severity due to antibody-dependent enhancement (ADE) of infection (9). Furthermore, although antiviral

66 therapies would be of great value in reducing the impact and global health burden of
67 flavivirus infections, no such antivirals are currently available.

68 Given the costly and time-consuming nature of development of novel antiviral drugs,
69 drug repurposing has emerged as a popular approach to accelerate the identification of safe
70 and effective antiviral therapeutics (10). This approach often involves screening of libraries
71 of approved and well-characterized drugs for compounds that inhibit viral infection or
72 associated pathogenesis, either directly via unanticipated inhibition of viral factors or
73 processes or indirectly through perturbation of host factors or pathways that are required for
74 the viral replication cycle. Given that the safety, bioavailability, half-life and, in most
75 instances, biological targets of these drugs have already been well-characterized, any
76 effective antiviral drugs identified via drug-repurposing screens could potentially be rapidly
77 re-positioned as antiviral therapeutics. In the context of flavivirus infection, several recent
78 screening studies have reported the identification of promising antiviral compounds amongst
79 libraries of approved and biologically active compounds, including known inhibitors of
80 flaviviral infection such as mycophenolic acid (MPA) and unexpected inhibitors of viral
81 replication such as the anti-helminthic drug niclosamide (11-14).

82 Here, we screened a library of 2,907 approved drugs and pharmacologically active
83 compounds for inhibitors of ZIKV infection in Huh-7.5 hepatoma cells. These screens
84 revealed 15 inhibitors of ZIKV infection, including previously identified antivirals such as
85 the nucleoside analogue thioguanine and novel antivirals such as the estrogen receptor (ER)
86 modulators raloxifene hydrochloride and quinestrol. Validation studies revealed that these ER
87 modulators similarly inhibit ZIKV, DENV-2 and WNV (Kunjin strain) infection at low
88 micromolar concentrations with minimal cytotoxicity. Mechanistically, these antiviral effects
89 appeared not to involve the major estrogen receptors, ER-α and ER-β, and could be
90 predominantly attributable to inhibition of viral RNA translation and/or replication. Taken

together, our study identifies ER modulators as inhibitors of flaviviral infections and supports their further exploration and improvement of their antiviral activity by medicinal chemistry as strategies to develop effective therapeutics to treat flavivirus infections.

RESULTS

Identification of candidate antiviral drugs via a high-throughput screen of approved drugs and pharmacologically active compounds. To identify novel inhibitors of ZIKV infection we developed a high-throughput cell-based assay of viral infection using an immunofluorescence readout in 96-well plate format. Specifically, compounds from a library comprised of 2,907 approved drugs and pharmacologically active compounds and vehicle (DMSO) controls were dispensed into 96-well black-walled imaging plates prior to plating of Huh-7.5 hepatoma cells to achieve a compound concentration of 10 µM. Huh-7.5 cells were chosen for the screen as their gene expression profile and growth properties have been characterised in numerous studies and they are susceptible to infection with a range of flaviviruses, including ZIKV (15, 16). Following plating, cells were then cultured for 24 hours prior to infection with ZIKV (strain PRVABC59; MOI ~3.6) and then cultured for a further 24 hours prior to fixation, immunofluorescent labelling using an antibody against the viral envelope protein (4G2) and automated fluorescence microscopy and image analysis to quantify the percentage of infected cells (Fig. 1A-B). The extended period (24 h) of compound exposure prior to infection was chosen to enable identification of additional compounds that may take time to accumulate or alter cellular gene expression profiles, metabolism or machinery to create an environment that is unfavourable to viral infection. The relatively short window of infection (24 h) and high multiplicity of infection were chosen to focus on inhibitors of early events in viral infection, such as entry, translation, establishment of viral replication complexes and viral RNA replication. For negative control wells that were

116 treated with DMSO vehicle alone (0.2% final concentration), 45.01% ± 4.40% and 51.66% ±
117 3.93% of cells were infected in the respective repeat screens. In this context, DMSO-treated
118 controls were associated with an average cell count of 5386.10 ± 457.58 cells in the imaged
119 area of each well in the first replicate screen (Fig. 1B, Table S1). As a positive control for
120 inhibition of infection, cells were treated with the polyether ionophore antibiotic
121 nanchangmycin at a final concentration of 1 μM, given a recent report that ZIKV infection is
122 potently inhibited by this drug (12). However, under the conditions of our screen this
123 treatment resulted in unacceptable levels of cellular cytotoxicity and a >50% reduction in cell
124 counts compared to vehicle controls (0.2% DMSO). Accordingly, robust Z' analysis was
125 applied for each plate and robust Z-scores for individual treatments were determined, which
126 uses the median and median absolute deviation (MAD) for calculations of screen robustness
127 and drug effects (17). The average robust Z' factors for each plate in the two replicate screens
128 were 0.87 ± 0.05 and 0.89 ± 0.05, respectively, indicating excellent robustness of the screens
129 and a good power to accurately identify compounds with significant effect sizes. With
130 regards to reproducibility of the screens, similar infection rates were observed for each
131 compound in the replicate screens, resulting in an R^2 correlation coefficient of 0.72 (Fig. 1C).
132 Similarly, analysis of robust Z-scores for each compound across the replicate screens
133 revealed an R^2 correlation coefficient of 0.66 (Fig. S1), indicating acceptable reproducibility
134 of the screens.

135 For our screens, hits were defined as having a robust Z-score of ≤ −2.0, an infection
136 rate of ≤ 50%, relative to that of the mean of DMSO controls, and a cell count of ≥ 50% of
137 that of the mean of DMSO controls, to exclude compounds that overtly affected cell viability.
138 According to these criteria, the repeat screens identified 53 and 56 hits, respectively, with 15
139 inhibitors that were common to both screens (Table 1). Amongst these common hits were
140 compounds that have previously been identified as inhibitors of flavivirus infection such as

141 thioguanine, a purine synthesis inhibitor, and imatinib, a tyrosine kinase inhibitor (11, 18).
142 Additional hits included the antimalarials dihydroartemesinin and artesunate, the
143 antihistamine azelastine HCl and the estrogen receptor modulators quinestrol and raloxifene
144 HCl (Table 1, Fig. 1B-C). Quinestrol and raloxifene hydrochloride (henceforth referred to as
145 'raloxifene') were chosen for further analysis given that little is known regarding the impact
146 of these compounds on flavivirus infections and our demonstration that estrogen receptor
147 modulators were highly represented amongst the hits identified in the individual repeat
148 screens, with additional related compounds that met the hit criteria in one of the repeat
149 screens including estradiol, ethinyl estradiol and estriol (Table S1).
150
151 **Dose-dependent inhibition of ZIKV, DENV2 and WNV (Kunjin) infection by quinestrol**
152 **and raloxifene.** We next sought to validate the antiviral activity of quinestrol and raloxifene
153 against ZIKV and determine whether these compounds were similarly efficacious against
154 related flaviviruses DENV-2 and WNV (Kunjin). For this we plated Huh-7.5 cells into black-
155 walled imaging plates containing the inhibitors to achieve a range of concentrations from 0.1
156 to 20 µM. Twenty-four hours later, cells were infected with ZIKV, DENV-2 or WNV
157 (Kunjin) at an M.O.I of ~3.6 and fixed 24 hours later, to mirror the conditions of the original
158 screens. Immunofluorescent labelling of the viral E protein and automated imaging and
159 analysis was then performed, prior to quantification of infection levels, relative to DMSO-
160 treated controls (Fig. 2). This revealed comparable low micromolar antiviral efficacy of
161 quinestrol against ZIKV, DENV-2 and WNV (Kunjin), with approximate IC_{50} values of 11.4
162 µM, 15.3 µM and 10.1 µM, respectively. Similarly, raloxifene displayed similar but slightly
163 more potent antiviral efficacy against ZIKV, DENV-2 and WNV (Kunjin), with approximate
164 IC50 values of 7.4 µM, 9.3 µM and 7.7 µM, respectively.

165 Given that infection of placental trophoblasts appears to be an important aspect of the
166 ability of ZIKV to infect the placenta and spread to the developing fetus in ZIKV-infected
167 pregnant mothers (19, 20), we also investigated the antiviral activity of quinestrol and
168 raloxifene in HTR8/SVneo cells that are derived from human first-trimester trophoblasts.
169 This revealed similar low micromolar antiviral activity of quinestrol against ZIKV, DENV-2
170 and WNV (Kunjin) (Fig. S2A). Consistent with results seen in Huh-7.5 cells, the antiviral
171 activity of raloxifene was slightly stronger than that of quinestrol, with approximate IC_{50}
172 values of 4.5 μM for each of ZIKV, DENV-2 and WNV (Kunjin) (Fig. S2B).

173 While the above immunofluorescence-based experiments demonstrated dose-
174 dependent antiviral effects of quinestrol and raloxifene towards these flaviviruses, it was not
175 clear whether the observed effects could be attributed to changes in viral entry, RNA
176 replication and/or infectious virus production. To explore these possibilities further, Huh-7.5
177 cells were infected with DENV-2 (MOI: ~0.05), washed extensively and returned to culture
178 for 48 h in the presence of a range of concentrations of quinestrol and raloxifene prior to
179 quantitation of intracellular DENV-2 RNA and virus infectivity in cell culture supernatants
180 (Fig. 3). This revealed dose-dependent reductions in viral RNA levels in response to both
181 quinestrol and raloxifene treatment (Fig. 3A). These effects were closely mirrored by
182 reductions in the production of infectious virus (Fig. 3B). Together, these results imply that
183 quinestrol and raloxifene inhibit early events in DENV-2 infection and/or viral RNA
184 replication but do not noticeably exert additional inhibitory effects on infectious virus particle
185 production.

186 Next, we sought to determine whether the antiviral effects of quinestrol and raloxifene
187 were attributable to cytotoxic and/or antiproliferative effects. For this, Huh-7.5 cells and
188 HTR8/SVneo cells were plated as above into 96-well plates containing a range of inhibitor
189 concentrations. Cells were then cultured for 48 hours prior to analysis of cell

viability/proliferation using a commercial resazurin-based cell viability assay (Fig. 4). This revealed that cell viability/proliferation was only appreciably inhibited at the highest drug concentrations (40-50 μM) in both cell types, with trends indicating that HTR8/SVneo cells are most sensitive to high concentrations of quinestrol. Whilst we were not able to determine CC_{50} values from this data for all conditions (i.e. $CC_{50} > 50$ μM), the CC_{50} of quinestrol in HTR8/SVneo cells was 36.3 μM, while the CC_{50} of raloxifene in Huh-7.5 cells was 38.7 μM. Similar effects were observed when an alternative ATP quantitation-based commercial cell viability assay was employed (Fig. S3), with quinestrol displaying CC_{50} values of 31.5 μM and 49.7 μM in HTR8/SVneo and Huh-7.5 cells, respectively. Taken together these results indicate that the estrogen receptor modulators quinestrol and raloxifene inhibit ZIKV, DENV-2 and WNV (Kunjin) infection at low micromolar concentrations in both Huh-7.5 and HTR8/SVneo cell lines in the absence of overt cellular cytotoxicity.

The antiviral activities of quinestrol and raloxifene are independent of cellular estrogen receptor expression. Both quinestrol and raloxifene target estrogen receptors. Quinestrol is the 3-cyclopentyl ether of ethinyl estradiol. Following ingestion and gastrointestinal absorption, it accumulates in adipose tissue and is slowly released, contributing to its long half-life. It is then readily metabolised to ethinyl estriol, a synthetic derivative of the natural estrogen estradiol that acts as an estrogen receptor (ER) agonist. It is commonly used in hormone replacement therapy and treatment of the symptoms of menopause and, less commonly, in the treatment of breast and prostate cancers. In contrast, raloxifene is a selective estrogen receptor modulator (SERM) that acts as an ER agonist in the cardiovascular system, bone and liver but acts as an ER antagonist in breast tissue and the endometrium. It is used in the prevention and treatment of osteoporosis and to reduce the risk of breast cancer development in at-risk individuals. Accordingly, we queried whether the

215 antiviral activities of quinestrol and raloxifene could be attributed to their actions upon ER-α
216 and/or ER-β signalling and we used Western blotting to assess ER-α and ER-β expression in
217 Huh-7.5 and HTR8/SVneo cell lines. This revealed that ER-α protein was not detectable in
218 either Huh-7.5 or HTR8/SVneo cell lines, whereas an ~60 kDa band corresponding to ER-α
219 was readily detected in lysates prepared from the ER-α-positive MCF-7 breast cancer cell
220 line (21) (Fig. 5A). Given controversy surrounding the specificities of various commercially
221 available antibodies that are reported to target ER-β and related conflicting reports
222 surrounding expression of ER-β in various cell lines (22, 23), we assessed ER-β expression in
223 Huh-7.5 cells and HTR8/SVneo cells using a validated ER-β-specific monoclonal antibody
224 (22), and as a positive control we used a stable LNCaP cell line that heterologously expresses
225 ER-β in response to doxycycline (23). As for ER-α, we found that ER-β protein was not
226 detectable in either Huh-7.5 or HTR8/SVneo cell lines, despite ready detection of ER-β in the
227 doxycycline-induced positive control cell line (Fig. 5B). While it is possible that these cell
228 types express very low levels of ER-α/β that are undetectable by Western blotting, our
229 analysis suggests that quinestrol- and raloxifene-mediated inhibition of flavivirus infection is
230 not dependent upon expression of ER-α or ER-β and instead involves an 'off-target'
231 mechanism of action.
232
233 **Quinestrol and raloxifene do not markedly alter viral protein localization.** To investigate
234 whether the antiviral effects of raloxifene coincided with changes in the subcellular
235 localization and/or the appearance of viral replication organelles and putative sites of virus
236 particle production, Huh-7.5 cells were simultaneously infected with DENV2-NS1-FLAG
237 and treated with 7.5 μM raloxifene or DMSO alone for 48 h prior to fixation,
238 immunofluorescent labelling and confocal fluorescence microscopy (Fig. 6). This DENV-2
239 derivative, which features a FLAG epitope insertion within the viral NS1 protein (24),

enabled immunofluorescent labelling of viral NS1 protein, double-stranded RNA (dsRNA) and either E or capsid proteins in the same samples. Whilst raloxifene treatment was predictably associated with a marked reduction in the overall level of infection in treated cell populations (not shown), there was no appreciable impact of raloxifene on viral E, capsid, NS1 or dsRNA localization. Similarly, the strong co-localization of NS1 and dsRNA at putative viral replication sites and the infrequent co-localization of dsRNA with capsid and E protein at putative viral assembly sites were not significantly altered by raloxifene treatment. Consistent with this, we did not observe any appreciable effects of quinestrol treatment on viral protein localization or co-localization under the same infection and treatment conditions (not shown). Taken together, the antiviral activity of these drugs against DENV-2 does not appear to be attributable to overt effects on viral protein localization in infected cells.

Quinestrol and raloxifene inhibit viral RNA replication

Next, we performed time-of-addition experiments to determine whether the antiviral effects of raloxifene and quinestrol were strongest when the drugs were added before, during or after the infection period (Fig. 7A, D, G). For these experiments a fluorescent reporter virus, DENV2-NS1-mScarlet (24), was used to enable simple live cell imaging by fluorescence microscopy and quantification of infection-associated fluorescence using a multi-mode plate reader. Interestingly, comparable inhibition of viral infection levels was observed regardless of whether drugs were applied to cells before (and after), during (and after) or only after the infection period (Fig. 7B-C, E-F, H-I). Accordingly, it is possible that these drugs disrupt an aspect of the virus replication cycle that is common to all of the treatment conditions, such as viral RNA replication. This is consistent with our earlier demonstration that treatment of Huh-7.5 cells with these drugs immediately following

264 infection with wildtype DENV-2 resulted in dose-dependent reductions in viral RNA levels
265 and commensurate reductions in infectious virus production (Fig. 3).

266 To further explore whether raloxifene and quinestrol impact upon viral RNA
267 replication and/or viral translation we employed luciferase-encoding DENV-2 and ZIKV
268 subgenomic replicons in transient viral replication assays. For this, Huh-7.5 cells stably
269 expressing *Firefly* luciferase were treated with drugs (5 μM) or DMSO carrier for 2 hours
270 prior to transfection with *in vitro* transcribed RNA for DENV-2 or ZIKV subgenomic
271 replicons and culture for 24-72 hours in the presence of drug or DMSO, as indicated (Fig.
272 8A). To gauge levels of *Renilla* luciferase activity that were associated with transfected
273 'input' RNA and enable assessment of the impact of these drugs on viral RNA translation,
274 replication-defective 'GND' or 'GAA' replicons were also employed. Although there were
275 no observable effects of drug treatments on cell appearance in these experiments, to account
276 for any impact of drug treatment on cell viability and/or proliferation, viral replication-
277 associated *Renilla* luciferase levels were normalized to cellular *Firefly* luciferase levels. As
278 shown in Fig. 8B, compared to controls, normalized DENV-2 RNA replication levels in
279 raloxifene-treated cells were ~10-fold lower across the first 48 hours post-transfection and
280 ~6-fold lower at 72 hours post-transfection. Strikingly, at 24 hours post-transfection, when
281 virally-encoded *Renilla* luciferase activity is comparable for wildtype and replication-
282 defective 'GND' replicons, raloxifene treatment was associated with a marked ~16-fold
283 reduction in 'GND'-associated luciferase activity compared to DMSO-treated 'GND'
284 controls. This suggests a substantial impact of raloxifene on viral polyprotein translation.
285 Consistent with this, raloxifene treatment resulted in a greater than 10-fold reduction in
286 virally-encoded luciferase levels for both replication-competent and replication-defective
287 'GAA' ZIKV subgenomic replicons (Fig. 8C).

288 In contrast, quinestrol treatment was associated with moderate ~2-4-fold inhibition of
289 DENV-2 subgenomic replicon-encoded luciferase activities and no appreciable changes in
290 virally-encoded luciferase activities for the replication-defective DENV-2 subgenomic
291 replicon (Fig. 8D), indicating that DENV-2 polyprotein translation is not inhibited by
292 quinestrol. While ZIKV subgenomic replicon-encoded luciferase activities were also
293 moderately reduced by quinestrol treatment, moderate quinestrol-mediated reductions in
294 luciferase activity were also observed for the replication-defective 'GAA' mutant replicon
295 (Fig. 8E). In this context, we also explored the possibility that quinesterol impacts directly
296 upon ZIKV NS5 RNA dependent RNA polymerase (RdRp) activity by using a fluorescence-
297 based assay of viral RNA replication and recombinant ZIKV NS5. This analysis revealed no
298 significant impairment of RdRp activity at 10 or 100 μM (Fig. S4).

299 To further examine the apparent impact of raloxifene on viral RNA translation, we
300 next investigated replication-defective subgenomic replicon-encoded *Renilla* luciferase
301 activity following short-term treatment with raloxifene or cycloheximide, a well-
302 characterised inhibitor of eukaryotic translational elongation. To simultaneously examine the
303 effects of these drugs on non-viral protein translation, the viral subgenomic replicon RNA
304 was co-transfected with a 5'-capped *Firefly* luciferase reporter mRNA. Following
305 transfection, cells were treated with raloxifene (5 μM) or cycloheximide (25 μg/ml) prior to
306 determination of *Renilla* luciferase (RLuc) and *Firefly* luciferase (FLuc) activities at 8, 16
307 and 24 h (Fig. 9A). Unexpectedly, FLuc activity was comparably inhibited, up to
308 approximately 13-fold, by both raloxifene and cycloheximide under these conditions (Fig.
309 9B-C, right panels). In contrast, virally-encoded RLuc activity was markedly reduced by
310 raloxifene treatment, up to approximately 75-fold, while cycloheximide treatment moderately
311 inhibited virally-encoded RLuc activity, up to approximately 5-fold (Fig. 9B-C, left panels).
312 Taken together, these results indicate that raloxifene treatment strongly impairs DENV-2 and

ZIKV RNA replication in a manner that may be attributable to inhibition of viral polyprotein translation and/or reduced stability of viral RNA. In contrast, quinestrol treatment modestly inhibits DENV-2 and ZIKV RNA replication and/or translation although the mechanism(s) involved remain unclear.

Next, we investigated whether hepatitis C virus (HCV) RNA replication is also sensitive to raloxifene and quinestrol, given its genetic relationship with flaviviruses as a member of the *Flaviviridae* family and previous reports that SERMs inhibit multiple aspects of the HCV replication cycle (25-27). For this, dose-response experiments were performed for raloxifene and quinestrol using Huh-7.5 cells harbouring a NanoLuc luciferase-tagged HCV subgenomic replicon. As shown, raloxifene and quinestrol treatments inhibited HCV RNA replication at low micromolar concentrations, with IC_{50} values of approximately 5.4 µM and 7.4 µM, respectively (Fig. S5A-B). For these experiments the NS5A inhibitor velpatasvir was used as a positive control (Fig. S5C). As expected, this treatment resulted in potent inhibition of HCV RNA replication, with an IC_{50} of ~41 pM.

DISCUSSION

In this study we developed and performed high-throughput screens to identify candidate antiviral drugs against ZIKV amongst a library of approved drugs and well-characterized pharmacologically active compounds. This led to the identification of 15 compounds that reproducibly inhibited ZIKV infection at 10 µM in the absence of overt cytotoxicity. Several similar recent high-throughput screening studies have been performed using libraries of FDA-approved drugs to identify safe and effective anti-ZIKV therapies amongst drugs that have already been approved for treatment of unrelated conditions and can therefore be considered for expedited trials for treatment of ZIKV-infected individuals (11-14). While our screens identified several hits that were also identified in similar previous screens, including

338 the purine analogue thioguanine (11), and the Bcr-Abl tyrosine kinase inhibitor imatinib (28),
339 to our knowledge our screens are the first to identify estrogen receptor modulators as
340 candidate antivirals for treatment of ZIKV infection.

341 Raloxifene is an archetypal SERM that was originally approved for use in the
342 treatment and prevention of postmenopausal osteoporosis and, later, to reduce the risk of
343 breast cancer development in at-risk individuals. It acts as an ER agonist in bone,
344 cardiovascular tissue and the liver and as an ER antagonist in breast tissue and the
345 endometrium. It is also classified as a cationic amphiphilic drug (CAD); a broad range of
346 compounds that feature a hydrophobic aromatic ring or ring system and a side-chain that is
347 hydrophilic and contains an ionisable amine functional group (29). CADs include other
348 SERMs, such as clomiphene and toremifene, and certain antimalarials, antidepressants,
349 antipsychotic drugs, antiarrhythmic drugs and cholesterol-lowering drugs (29). Interestingly,
350 many CADs display antiviral activities against a range of viruses including Ebola virus
351 (EBOV), DENV, ZIKV, HCV, Middle East respiratory syndrome coronavirus (MERS-CoV)
352 and Severe Acute Respiratory Syndrome Coronavirus (SARS-CoV) and in many instances
353 these antiviral effects have been attributed to the pH-dependent accumulation of CADs in late
354 endosomes/lysosomes (LE/Lys) and subsequent enlargement of these vesicles and disruption
355 of their involvement in the replication cycles of these viruses (25, 26, 29-34). (31,
356 32)(35)(36)

357 While many of the studies of the antiviral activity of CADs have focussed upon
358 inhibition of viral fusion (31, 32, 35, 36), the strongest antiviral effects of raloxifene in our
359 studies involved the use of ZIKV and DENV-2 subgenomic replicons. This suggests that
360 impairment of virus entry/fusion is not the major antiviral mechanism of raloxifene against
361 these viruses and instead disruption of viral RNA replication/translation predominates. We
362 hypothesise that the antiviral impact of raloxifene on flavivirus RNA replication/translation

363 may be attributable to its alteration of endosomal cholesterol content, trafficking and/or
364 biogenesis, in a similar manner to U18666A, another CAD which inhibits lysosomal
365 cholesterol export via targeting Niemann-Pick C1 (NPC1) (37), and inhibits DENV RNA
366 replication and HCV RNA replication via perturbation of cholesterol recruitment to viral
367 replication organelles (38, 39). While previous studies have shown that raloxifene and other
368 SERMs disrupt cholesterol trafficking in macrophages and other cell types (29, 40), it will be
369 important to investigate whether the antiviral effects of raloxifene against flaviviruses that we
370 have observed are attributable to perturbation of LE/Lys cholesterol content and trafficking.
371 Of note, while this manuscript was in preparation, Tohma *et al* reported that the SERMs
372 cyclofenil, clomiphene and tamoxifen also inhibit DENV and ZIKV replication and, in
373 particular, infectious virus production (41). While our study indicates that raloxifene
374 predominantly disrupts viral RNA replication/translation, consistent with our findings,
375 Tohma *et al* also found that the antiviral effects of SERMs appeared to be independent of ER
376 signalling.

377 While both raloxifene and quinestrol target estrogen receptors, the antiviral activity of
378 quinestrol that we observed also appears to be independent of its effects on ER signalling.
379 While quinestrol is not classified as a SERM or a CAD, it is possible that its high
380 lipophilicity and accumulation in lipid storage vesicles may contribute towards its antiviral
381 activity via perturbation of host cell lipid trafficking, given the intimate relationship between
382 flaviviruses and host cell lipids (42). Further studies are required to dissect the antiviral
383 mechanisms of quinestrol and structurally related estrogen receptor agonists. Additionally,
384 while we have observed similar antiviral effects of quinestrol and raloxifene against ZIKV,
385 DENV-2 and WNV/KUNV isolates, further studies are required to determine whether there
386 are flavivirus-, DENV serotype- and/or viral isolate-dependent differences in the antiviral

activity of these drugs and whether the antiviral effects against *Flaviviridae* family viruses observed in this study extend to other unrelated viruses.

Taken together, our high-throughput screens for inhibitors of ZIKV infection amongst approved and pharmacologically active compounds identified 15 compounds from a broad variety of drug classes as candidate antiviral drugs that warrant further investigation. Whilst some of these compounds have been identified in previous antiviral screening efforts (e.g. thioguanine and imatinib) and others are not suitable for oral or systemic administration and absorption (e.g. dequalinium chloride), we propose that the antiviral activities and mechanisms of action of estrogen receptor modulators raloxifene and quinestrol deserve further investigation in regards to the urgent and unmet need for safe and effective antiviral therapeutics to treat flavivirus infections. In particular, given the growing appreciation that SERMs and other CADs have broad spectrum antiviral activity against a range of viral pathogens (29, 43), raloxifene and existing and novel structurally-related analogues may warrant investigation as candidate antiviral agents against pathogenic flaviviruses. Although the low micromolar antiviral activity of raloxifene described here is several hundred times higher than reported plasma concentrations in postmenopausal women following a single orally-ingested 60 mg dose (~1-3 nM), the relatively strong safety profile of raloxifene and structurally-related SERMs support the further exploration of these drugs as future antiviral therapeutics. We suggest that medicinal chemistry efforts to develop raloxifene analogues and/or derivatives with improved potency and safety profiles may yield safe and effective antiviral therapeutics that can be employed in treatment of flavivirus infections.

MATERIALS AND METHODS

Cell Culture

411 Huh-7.5 cells (44), and Vero cells were generously provided by Charles Rice (Rockefeller
412 University, New York, USA) and Jillian M. Carr (Flinders University, Adelaide, Australia),
413 respectively. Both of these cell lines were cultured in Dulbecco's modified Eagle medium
414 (DMEM; Life Technologies cat. no. 12430) supplemented with 100 U/ml penicillin, 100
415 µg/ml streptomycin and 10% fetal bovine serum (FBS), as described previously (45). C6/36
416 cells were also generously provided by Jillian M. Carr (Flinders University) and were
417 cultured as described previously (24, 46). Huh-7.5+FLuc cells, which stably express *Firefly*
418 luciferase, were maintained in complete DMEM containing blasticidin (5 µg/ml) and have
419 been described previously (45). Huh-7.5+SGR/5A-NLuc (E7) cells, which stably harbour a
420 NanoLuc-encoding subgenomic HCV replicon have been described previously (47), and were
421 cultured in complete DMEM containing blasticidin (5 µg/ml). The anti-E hybridoma cell line
422 D1-4G2-4-15 ('4G2') was purchased from ATCC and was cultured in Hybri-Care Medium
423 (ATCC) supplemented with sodium bicarbonate and 10% FBS, as per manufacturer's
424 recommendations. LNCaP cells expressing ER-β in a doxycycline-inducible manner
425 (LNCaP+ERβ) were generously provided by Jean Winter and Wayne Tilley (University of
426 Adelaide, Adelaide, Australia) on behalf of Jason Carroll (University of Cambridge,
427 Cambridge, UK) and were cultured in DMEM supplemented with 100 U/ml penicillin, 100
428 µg/ml streptomycin and 10% FBS. FBS and cell culture plasticware were purchased from
429 Sigma-Aldrich. All other cell culture media and additives were purchased from Thermo
430 Fisher Scientific.
431

432 **Viruses and Plasmids**

433 ZIKV (PRVABC59; Puerto Rico, 2015) was originally obtained from ATCC. WNV (Kunjin
434 strain NSW2011) was generously provided by Karla J. Helbig (La Trobe University,
435 Melbourne, Australia). Plasmid pFK-DVs, which contains a full-length DENV-2 genome

436 (strain 16681), and subgenomic *Renilla* luciferase reporter-encoding replicon constructs for
437 DENV-2 (pFK-sgDVs-R2A and pFK-sgDVs-R2A-GND) and ZIKV (pFK-synZIKV-sgR2A-
438 H/PF/2013 and pFK-synZIKV-sgR2A-H/PF/2013-GAA) were generously provided by Ralf
439 Bartenschlager (University of Heidelberg, Heidelberg, Germany) (48, 49). Plasmids pFK-
440 DVs-NS1-FLAG and pFK-DVs-NS1-mScarlet and the derivative viruses were described
441 recently (24). To initiate virus replication for the above cloned viral genome constructs,
442 plasmids were first linearized with *Xba*I (DENV-2 constructs) or *Xho*I (ZIKV constructs)
443 before use as templates in *in vitro* transcription reactions using an mMessage mMachine SP6
444 Transcription kit or mMessage mMachine T7 Transcription kit (Thermo Fisher Scientific) for
445 DENV-2 or ZIKV constructs, respectively. Following DNase treatment to digest plasmid
446 template DNA, *in vitro*-transcribed viral RNA was purified using TRIsure (Bioline) and
447 transfected into Huh-7.5 cells using DMRIE-C Reagent (Thermo Fisher Scientific), as
448 described previously (45). Infectious viruses were amplified in C6/36 cells, clarified by
449 centrifugation at 500 × *g* for 10 min at 4°C, aliquoted and stored at -80°C. Virus infectivity
450 was determined as described below.
451

452 **Plaque Assays and Focus-Forming Assays of Viral Infectivity**

453 Virus infectivity was measured by plaque assays using Vero cells, as follows. Cells were
454 seeded in 12-well trays at 2×10^5 cells/well and cultured overnight prior to infection with 0.5
455 ml of 10-fold serial dilutions of virus in normal media. Following incubation for 1 h, virus
456 was removed and replaced with 1 ml of 1.5% high viscosity sodium carboxymethylcellulose
457 (Sigma-Aldrich) dissolved in serum-free DMEM. Cells were then returned to culture for 5
458 days prior to addition of 1 ml of 10% buffered formalin and fixation at 4°C overnight. Fixed
459 cell monolayers were then washed 3 times with water, stained with 1% crystal violet solution
460 for 20 min at room temperature and washed extensively with water prior to enumeration of

plaques and determination of the infectivity of original samples, expressed as plaque-forming units per millilitre (PFU/ml). Focus-forming assays were performed using Huh-7.5 cells and anti-E immunofluorescent staining, as described recently (24).

Drug Library Screening and Automated Imaging

In our screen the Open Access Drugs library from Compounds Australia (Griffith University) was employed. This library is comprised of the MicroSource Spectrum FDA-approved drug library of 2,560 compounds and 347 additional pharmacologically active 'in house' compounds (2,907 compounds in total), dissolved in DMSO to 5 mM. Compounds and controls (DMSO and Nanchangmycin [Selleck Chemicals] at 0.5 mM) were dispensed by Compounds Australia into 96-well black wall, clear bottom imaging plates (Greiner Bio-One CELLSTAR 96W Microplates; cat. no. 655090) at 300 nL/well. Plates were then sealed and shipped at room temperature to the screening facility (CellScreen SA, Flinders University), where a BioTek EL406 Washer Dispenser was used to dispense 7,500 Huh-7.5 cells per well in 150 µL of complete DMEM media (from a cell suspension of 5×10^4 cells/mL) to achieve a final drug concentration of 10 µM. Cells were then returned to culture for 24 h prior to addition of 50 µL of ZIKV PRVABC59 diluted in media to achieve an MOI of ~3.6. Following culture for a further 24 h, the media was removed and cells were fixed with ice-cold methanol:acetone (1:1) at 4 °C for 10 min. Following removal of the fixative and washing with PBS, cell monolayers were blocked with 5% BSA in PBS (50 µL/well) for 30 min at room temperature. The blocking solution was then removed and 40 µL/well of anti-E hybridoma cell supernatant diluted 1:5 in PBS/1% BSA was added and incubated at 4°C overnight. Following a PBS wash step, cell monolayers were then incubated for ~2 h at 4°C with 40 µL/well of AlexaFluor-488-conjugated anti-mouse IgG (Life Technologies) diluted 1:200 in PBS/1% BSA. Cells were then washed, incubated with DAPI (Sigma-Aldrich, 1

486 μg/ml in PBS) for ~30 min at room temperature and washed again. Automated imaging was
487 performed using an Operetta High Content Imaging and Analysis System (PerkinElmer).
488 Briefly, for each well 4 separate fields were imaged for AlexaFluor-488 and DAPI
489 fluorescence using a 10× objective. Image analysis was performed using Harmony and
490 Columbus software (PerkinElmer), whereby infected cells were identified on the basis of
491 AlexaFluor-488 fluorescence intensity thresholds that were established using negative control
492 (DMSO)- and compound-treated wells and cell segmentation that was performed on the basis
493 of nuclear DAPI-associated fluorescence and cytoplasmic AlexaFluor-488-associated
494 fluorescence. As detailed in the Results, robust Z' analysis was performed for each plate and
495 robust Z-scores for each compound treatment were calculated, based upon the median and
496 median absolute deviation (MAD) for calculations of screen robustness and drug effects (17).
497 Hits were defined as having a Z-score of ≤ -2.0, a ZIKV infection rate of ≤ 50% compared to
498 DMSO-treated controls and a cell count of ≥ 50% of that of DMSO-treated controls.
499 Validation (dose-response) experiments were performed using the same experimental
500 workflow, with the exception that cells were plated into 96-well imaging plates and allowed
501 to adhere for 3 h prior to replacement of media with media containing compounds diluted to a
502 range of different concentrations (0.1 μM, 0.5 μM, 1 μM, 2.5 μM, 5 μM, 7.5 μM, 10 μM, 15
503 μM and 20 μM) with DMSO at a fixed final concentration of 0.8% (v/v). Cells were infected
504 24 h later (MOI ~3.6), cultured for a further 24 h and fixed and processed for
505 immunofluorescence and analysis, as detailed above. IC_{50} values for each compound were
506 determined using variable slope (four parameters) least squares fit analysis in Prism 8
507 (GraphPad Software).
508
509 **Antibodies, Chemicals and Compounds**

510 Mouse anti-E monoclonal antibody (mAb) 4G2 was prepared from D1-4G2-4-15 hybridoma
511 cells, cultured as described above. Anti-dsRNA mouse monoclonal antibody (mAb) 3G1
512 (IgM) hybridoma cell supernatant was generously provided by Roy Hall (University of
513 Queensland, Brisbane, Australia). Mouse anti-capsid mAb 6F3.1 was generously provided by
514 John Aaskov (Queensland University of Technology, Brisbane, Australia). Rabbit anti-FLAG
515 mAb (D6W5B) was purchased from Cell Signaling Technology. Rabbit anti-ER-α mAb
516 (60C) was purchased from Merck-Millipore. Mouse anti-ER-β mAb (PPZ0506) was
517 purchased from R&D Systems. Mouse anti-β-actin mAb (AC-74) was purchased from
518 Sigma-Aldrich. AlexaFluor 488-, 555- and 647-conjugated secondary antibodies and HRP-
519 conjugated secondary antibodies were purchased from Thermo Fisher Scientific.

520 Nanchangmycin and raloxifene HCl were purchased from Selleck Chemicals and
521 dissolved in DMSO to 10 mM and 20 mM, respectively, aliquoted and stored at -80°C.
522 Quinestrol was purchased from Cayman Chemical, dissolved in DMSO to 20 mM, aliquoted
523 and stored at -80°C. Cycloheximide ready-made solution (100 mg/ml in DMSO) was
524 purchased from Sigma-Aldrich and stored at 4°C. DAPI (4',6-Diamidino-2-phenylindole
525 dihydrochloride) and Hoechst (bisBenzimide H 33342 trihydrochloride) DNA dyes and
526 doxycycline hydrochloride were purchased from Sigma-Aldrich, dissolved in sterile water to
527 1 mg/mL and stored at 4°C.

528

529 **Quantification of Viral RNA by qRT-RCR**

530 Total cellular RNA extraction and quantification of DENV-2 RNA via qRT-PCR was
531 performed essentially as described (46). Briefly, following washing with PBS, RNA was
532 extracted from near-confluent cells in 12-well trays using NucleoZOL (Macherey-Nagel),
533 according to manufacturer's instructions. DENV-2 RNA was quantified by qRT-PCR using
534 Luna Universal One-Step RT-qPCR Kit (New England Biolabs) in 384-well plates, according

535 to manufacturer's instructions. Briefly, for each sample and primer pair 10 µl reactions were
536 prepared in technical duplicate, each containing 62.5 ng of isolated RNA (2.5 µl at 25 ng/µl),
537 0.2 µl of each primer at 20 µM (0.4 µM final concentration; DENV-2 sense primer: 5'-ATC
538 CTC CTA TGG TAC GCA CAA A-3'; DENV-2 antisense primer: 5'-CTC CAG TAT TAT
539 TGA AGC TGC TAT CC-3'; RPLPO sense primer: 5'-AGA TGC AGC AGA TCC GCA T-
540 3'; RPLPO antisense primer: 5'-GGA TGG CCT TGC GCA-3'), 1.6 µl nuclease-free water
541 and 0.5 µl Luna WarmStart RT Enzyme Mix. Reactions were performed using an Applied
542 Biosystems QuantStudio 7 Flex Real-Time PCR System using the following program: 55°C
543 for 10 min, 95°C for 1 min and 40 cycles of the following: 95°C for 15 s, 60 °C for 1 min.
544 Melt curve analysis was performed using default settings of the instrument. DENV-2 RNA
545 levels were expressed as a percentage of those of DMSO-treated controls, following
546 normalization to RPLPO mRNA, using the ΔΔ*C*t method.
547

548 **Confocal Fluorescence Microscopy and Live Cell Imaging**

549 For confocal fluorescence microscopy, Huh-7.5 cells were seeded into (#1.5H) µ-Slide 8-well
550 glass bottom chamber slides (Ibidi) that were pre-coated with 0.2% (w/v) gelatin at 10,000
551 cells/well and returned to culture overnight. Cells were then treated with media containing
552 raloxifene (7.5 µM), quinesterol (7.5 µM) or DMSO carrier (0.1% [v/v]), infected with
553 DENV2-NS1-FLAG (MOI ~0.1) and returned to culture for 48 h. Cells were then fixed for 5
554 minutes at 4 °C with ice-cold acetone:methanol (1:1), washed with PBS and blocked with 5%
555 BSA/PBS for 30 mins. Cells were then incubated with primary antibody mixtures containing
556 rabbit anti-FLAG (1 in 200) and either mouse anti-E hybridoma supernatant (1 in 5) or mouse
557 anti-capsid hybridoma supernatant (1 in 5) diluted in PBS/1% BSA. Cells were then washed
558 with PBS and incubated for 1 h at 4°C with Alexa Fluor 647-conjugated anti-mouse IgG (1 in
559 200) and Alexa Fluor 488-conjugated anti-rabbit IgG (1 in 200) diluted in 1% BSA/PBS.

560 Following PBS wash steps, cells were then labelled by indirect immunofluorescence, as
561 above, using anti-dsRNA hybridoma supernatant (1 in 5) followed by Alexa Fluor 555-
562 conjugated anti-mouse IgM (1 in 200). Cells were then washed, labelled for 15 mins with
563 DAPI (1 µg/mL) diluted in PBS and washed again with PBS prior to replacement with
564 VECTASHIELD Antifade Mounting Medium (Vector Laboratories) and immediate imaging.
565 Specificity of labelling was confirmed using mock-infected cells and infected cells that were
566 labelled using irrelevant isotype control primary antibodies (BD Pharmingen) and omission
567 of primary antibody as a control for anti-dsRNA labelling (not shown). Confocal imaging
568 was performed using an Olympus FLUOVIEW FV3000 confocal microscope system using a
569 60× NA 1.42 oil immersion objective and images were processed using NIS Elements AR
570 v.3.22 (Nikon) and Photoshop 6.0 (Adobe) software.

571 For live cell imaging and plate reader-based quantitation of cellular fluorescence in
572 live cells, Huh-7.5 cells were seeded into black wall 96-well imaging plates in phenol red-
573 free media at 7,500 cells/well and cultured overnight prior to drug treatment and/or infection
574 with DENV2-NS1-mScarlet, as appropriate. At the completion of the time-course, cells were
575 labelled with Hoechst 33342 (1 µg/mL) in phenol red-free media for 30 mins at 37°C. Cells
576 were then washed once with normal media and an optical adhesive film was applied to the
577 plate before quantitation of mScarlet-associated fluorescence in each well using a PHERAstar
578 FS multi-mode microplate reader (BMG Labtech) equipped with a 540/590 nm fluorescence
579 intensity module using 'well scanning' mode.

580

581 **Cell Viability Assays**

582 Cell viability assays were performed using PrestoBlue Cell Viability Reagent (Thermo Fisher
583 Scientific), according to manufacturer's instructions. Viability-associated fluorescence was
584 quantified using a PHERAstar FS multi-mode microplate reader (BMG Labtech) and the

585 540/590 nm fluorescence intensity module. Alternatively, cells were cultured in 96-well
586 white polystyrene cell culture plates (Costar cat. no. 3917), treated with drugs, as appropriate,
587 and cell viability was measured using a CellTiter-Glo Luminescent Cell Viability Assay
588 (Promega) as per manufacturer's instructions using a GloMax-96 luminometer (Promega).
589 Where possible CC_{50} values for each compound were determined using variable slope (four
590 parameters) least squares fit analysis in Prism 8 (GraphPad Software).
591

592 **Quantitative RdRp Assays**

593 To generate recombinant ZIKV RdRp, a pET24+ plasmid (NEB) containing the ZIKV RdRp
594 coding sequence minus the N-terminal methyltransferase domain (nts 8,466-10,375 of strain
595 MR766 [GenBank Accession LC002520]) was first transformed into T7 Express competent
596 *E.coli* (NEB). ZIKV RdRp was overexpressed in *E. coli* by the addition of 0.5 mM isopropyl-
597 β-thiogalactopyranoside, and overnight incubation (16°C, 200 rpm). RdRp purification was
598 performed by chemically lysing *E. coli* pellets and then enriching the hexahistidine-tagged
599 RdRp using Ni-NTA resin on a BioScale Mini Profinity IMAC Cartridge (Bio-Rad).
600 Quantitative *in vitro* fluorescence-based assays of *de novo* RdRp activity were performed
601 using PicoGreen (Thermo Fisher Scientific) to detect formation of dsRNA from a poly(U)
602 RNA template, as described previously (50, 51).
603

604 **Immunoblotting and Luciferase Assays**

605 Immunoblotting was performed essentially as described (52). Briefly, cell monolayers were
606 washed with PBS and lysed in ice-cold NP-40 lysis buffer (1% NP-40, 150 mM NaCl, 50
607 mM Tris [pH 8.0]) containing protease inhibitor cocktail (Sigma-Aldrich). Samples were then
608 homogenized using a 25-gauge needle/syringe and clarified by centrifugation (10,000 ×*g*, 5
609 min at 4°C). For each sample ~50 µg of protein was separated by SDS-PAGE and transferred

610 to Hybond ECL nitrocellulose membrane (GE Healthcare). Following blocking for 1 h at
611 room temperature in TBS-Tween 20 (0.1%; TBS-T) containing 5% skim milk, membranes
612 were incubated overnight in anti-ERα (1 in 500), anti-ERβ (1 in 500) or anti-β-actin (1 in
613 10,000) antibodies diluted in TBS-T containing 1% skim milk. Membranes were then washed
614 in TBS-T (3 times for 10 min each) and incubated for 1 h at room temperature in HRP-
615 conjugated anti-mouse or anti-rabbit IgG secondary antibodies diluted in TBS-T containing
616 1% skim milk. Following extensive washing with TBS-T, membranes were developed using
617 SuperSignal West Femto Maximum Sensitivity Substrate (Thermo Fisher Scientific) and
618 imaged using a ChemiDoc MP imaging system (Bio-Rad).

619 Transient viral replication assays using subgenomic DENV-2 and ZIKV replicons
620 were performed as follows. Huh-7.5+FLuc cells were treated with drugs or DMSO as
621 indicated for 2 h prior to transfection with *in vitro* transcribed RLuc-encoding replicon RNA
622 using DMRIE-C (Thermo Fisher Scientific), according to manufacturer's instructions.
623 Following incubation for 3 h, transfection complexes were removed and cells were either
624 lysed in Passive Lysis Buffer (Promega) or returned to culture for 24 h, 48 h or 72 h in media
625 containing drug or DMSO, as appropriate, prior to lysis. Dual luciferase assays (Promega)
626 were then performed according to manufacturer's instructions using a GloMax-96
627 luminometer. *Renilla* luciferase (RLuc) values were normalized to *Firefly* luciferase (FLuc)
628 values and expressed as a percentage of average 3 h 'input' values for each group. Assays of
629 viral translation were performed as above, with the exception that Huh-7.5 cells were co-
630 transfected with equal amounts of RLuc-encoding replication-defective subgenomic replicon
631 RNA and 5'-capped FLuc mRNA, prepared using the FLuc Control Template provided in the
632 HiScribe T7 High Yield RNA Synthesis Kit (New England Biolabs). Following collection of
633 samples at 4, 8, 16 and 24 h post-transfection, dual luciferase assays were performed and
634 individual RLuc and FLuc values were expressed as a percentage of corresponding average 4

h 'input' values. For HCV replicon experiments, Huh-7.5+SGR/5A-NLuc (E7) cells harbouring a stable NanoLuc-encoding subgenomic replicon were treated with drugs at a range of concentrations and cultured for 48 h prior to lysis in Passive Lysis Buffer (Promega) and determination of luciferase activity using a Nano-Glo Luciferase Assay System (Promega), as per manufacturer's instructions.

ACKNOWLEDGEMENTS

We are grateful to Ralf Bartenschlager (University of Heidelberg), Charles Rice (The Rockefeller University), Jillian Carr (Flinders University), Roy Hall (University of Queensland), John Aaskov (Queensland University of Technology), Jean Winter and Wayne Tilley (University of Adelaide, Adelaide, Australia), Jason Carroll (University of Cambridge, Cambridge, UK) and Karla Helbig (La Trobe University, Melbourne, Australia) for generously providing reagents, as detailed in the Materials and Methods. We thank Jane Sibbons (Adelaide Microscopy, University of Adelaide) for assistance with confocal microscopy, Emma Harding (UNSW) for assistance with RdRp assays and Steve Johnson (University of Adelaide) for performing RNA extractions for qRT-PCR experiments. We also thank Moana Simpson, Rebecca Lang and other staff members from Compounds Australia at Griffith University for providing compound libraries in assay-ready plates. This work was funded by grants from the Channel 7 Children's Research Foundation (171433 to N.S.E.) and the National Health and Medical Research Council (NHMRC) (1163662 to N.S.E. and 1027641 to M.R.B.). The funders had no role in the study design, data collection and interpretation, or the decision to submit the work for publication.

FIGURE LEGENDS

659 **FIG 1.** Identification of inhibitors of ZIKV infection amongst a library of FDA-approved and
660 pharmacologically active compounds using an immunofluorescence-based assay. (A) Drug
661 screening timeline and workflow. Huh-7.5 cells were plated into 96-well imaging plates
662 containing compounds to achieve a final drug concentration of 10 µM. Cells were then
663 cultured for 24 h and infected with ZIKV (PRVABC59, MOI: ~3.6). Cells were then cultured
664 for a further 24 h, fixed, labelled by anti-E indirect immunofluorescence (green),
665 counterstained with DAPI (blue and red in upper and lower micrographs, respectively) and
666 analysed by automated fluorescence microscopy. (B) Graphical representation of ZIKV
667 infection rates and cell numbers for each compound in the first screen replicate. (C) Screen
668 reproducibility. Infection rates for each of the replicate screens were plotted against one
669 another and the R^2 correlation was determined. For (B) and (C), red spheres represent
670 compounds that met the hit selection criteria (see Materials and Methods), while the data
671 points for raloxifene HCl and quinestrol are also indicated (box-lines).
672
673 **FIG 2.** Dose-response analysis of the antiviral effects of quinestrol and raloxifene. Huh-7.5
674 cells were treated with quinestrol or raloxifene at a range of concentrations, as indicated, for
675 24 h prior to infection with ZIKV (A), DENV-2 (B) or WNV-KUNV (C) at an MOI of ~3.6.
676 Cells were then cultured for 24 h and processed for immunofluorescence and automated
677 imaging analysis to determine infection rates, relative to DMSO-treated (carrier) controls. For
678 quinestrol, IC_{50} values were 11.4 µM, 15.3 µM and 10.1 µM against ZIKV, DENV-2 and
679 WNV-KUNV, respectively. For raloxifene, IC_{50} values were 7.4 µM, 9.3 µM and 7.7 µM
680 against ZIKV, DENV-2 and WNV-KUNV, respectively. Data are means ± S.D. (n = 3-4),
681 representative of at least two similar repeat experiments. Fitted curves represent best fits for
682 IC_{50} calculations.
683

684 **FIG 3.** Dose-response analysis of the antiviral effects of quinestrol and raloxifene on DENV-
685 2 RNA and infectious virus production. Huh-7.5 cells were infected with DENV-2 (MOI:
686 ~0.05) for 2 hours, washed twice with PBS and returned to culture for 48 h in the presence of
687 quinestrol (left panels) or raloxifene (right panels) at the indicated concentrations. Samples
688 were then collected for analysis of: (A) intracellular DENV-2 RNA levels by qRT-PCR
689 (normalised to the housekeeping gene RPLPO and expressed as a percentage of DMSO-
690 control values) and; (B) infectious virus levels in cell culture supernatants (determined by
691 focus-forming assays). Data are means ± S.D. (n = 3).
692
693 **FIG. 4.** Dose-response analysis of the impact of quinestrol and raloxifene on cell viability.
694 Huh-7.5 cells (A) or HTR-8 cells (B) were treated with quinestrol or raloxifene at the
695 indicated concentrations (0.5 – 50 μM) for 48 h prior to analysis of viability using a
696 resazurin-based fluorescent cell viability assay. Data are means ± S.D. (*n* = 4), representative
697 of similar repeat experiments.
698
699 **FIG. 5.** Western blot analysis of ERα and ERβ protein expression in Huh-7.5 and HTR-
700 8/SVneo cells. Whole cell lysates were prepared from the indicated cell lines and subjected to
701 SDS-PAGE and Western blotting using antibodies against ERα (A) and ERβ (B). Lysates
702 from MCF-7 cells and LNCaP cells heterologously expressing ERβ were used as positive
703 controls for expression of ERα and ERβ, respectively. β-actin served as a loading control.
704
705 **FIG. 6.** Raloxifene does not appreciably alter the localization or appearance of DENV-2 viral
706 RNA replication or assembly sites. Huh-7.5 cells were simultaneously infected with DENV2-
707 NS1-FLAG (MOI: ~0.1) and treated with raloxifene (7.5 μM) or DMSO as a carrier control.
708 At 48 h post-infection, cells were fixed and processed for indirect immunofluorescent

709 labelling of combinations of (A) NS1 (green), dsRNA (red) and E (cyan) or (B) NS1 (green),
710 dsRNA (red) and Capsid (cyan). DAPI (grey in merged images) was used to stain nuclear
711 DNA. Scale bars in merged images are 10 µm and 5 µm for main images and 'insets',
712 respectively.
713
714 **FIG. 7.** Time-of-addition analysis of the antiviral effects of raloxifene and quinestrol against
715 DENV-2. Huh-7.5 cells were treated with raloxifene (5 or 10 µM), quinestrol (5 or 10 µM) or
716 DMSO (control) and infected with DENV2-NS1-mScarlet (MOI: ~0.01) for 3 h, according to
717 the timelines depicted in (A), (D) and (G). Cells were then labelled with Hoechst 33342 and
718 imaged by live cell imaging, as depicted in micrographs shown in (B), (E) and (H). Plates
719 were then processed for quantification of NS1-mScarlet-associated fluorescence using a
720 multi-mode plate reader. Graphs (C, F and I) show infection-associated fluorescence levels,
721 expressed as a percentage of those of DMSO-treated controls. Data are means + S.D. (n = 4),
722 representative of similar repeat experiments. Asterisks (* $P < 0.05$; ** $P < 0.01$; *** $P <$
723 0.001) indicate statistically significant differences compared to DMSO-treated controls, as
724 determined by unpaired Student's *t*-tests.
725
726 **FIG. 8.** Inhibition of DENV-2 and ZIKV viral RNA replication in response to raloxifene and
727 quinestrol treatment. (A) Timeline depicting treatment of Huh-7.5+FLuc cells with raloxifene
728 ('RALOX') or quinestrol ('QUIN') at 5 µM for 2 h prior to and 24-72 h following
729 transfection with *in vitro*-transcribed viral RNA for *Renilla* luciferase-encoding subgenomic
730 replicons (SGR). For cells transfected with sgDV.R2A replicon RNA (B and D) or
731 sgZV.R2A replicon RNA (C and E), samples were harvested at 3, 24, 48 and 72 h post-
732 transfection, as indicated, and normalised luciferase activities (RLuc/FLuc) were determined

733 and expressed as a percentage of average values for each group at 3 h time-points. Data are
734 means + S.D. (n = 4), representative of similar repeat experiments.
735
736 **FIG 9.** Inhibition of viral RNA translation by raloxifene. (A) Timeline depicting co-
737 transfection of Huh-7.5 cells with the indicated replication-defective subgenomic replicon
738 RNA (sgDV.R2A [GND] or sgZV.R2A [GAA]) and FLuc mRNA and either immediate
739 harvest of samples (4 h) or culture for 8, 16 or 24 h with media containing DMSO (0.05%
740 [v/v]), cycloheximide ('CHX'; 25 µg/ml) or raloxifene ('RALOX'; 5 µM) prior to sample
741 collection and analysis by dual luciferase assay. (B) Quantification of sgDV.R2A (GND)-
742 encoded RLuc activity (left panel) and FLuc activity (right panel), expressed as a percentage
743 of average 4 h values. (C) Quantification of sgZV.R2A (GAA)-encoded RLuc activity (left
744 panel) and FLuc activity (right panel), expressed as a percentage of average 4 h values. Data
745 are means ± S.D. (n = 4).
746
747 **REFERENCES**

748 1. Bhatt S, Gething PW, Brady OJ, Messina JP, Farlow AW, Moyes CL, Drake JM,
749 Brownstein JS, Hoen AG, Sankoh O, Myers MF, George DB, Jaenisch T, Wint GR,
750 Simmons CP, Scott TW, Farrar JJ, Hay SI. 2013. The global distribution and burden
751 of dengue. Nature 496:504-507.
752 2. Pierson TC, Diamond MS. 2018. The emergence of Zika virus and its new clinical
753 syndromes. Nature 560:573-581.
754 3. Mead PS, Hills SL, Brooks JT. 2018. Zika virus as a sexually transmitted pathogen.
755 Curr Opin Infect Dis 31:39-44.
756 4. Cugola FR, Fernandes IR, Russo FB, Freitas BC, Dias JL, Guimaraes KP, Benazzato
757 C, Almeida N, Pignatari GC, Romero S, Polonio CM, Cunha I, Freitas CL, Brandao

758 WN, Rossato C, Andrade DG, Faria Dde P, Garcez AT, Buchpigel CA, Braconi CT,
759 Mendes E, Sall AA, Zanotto PM, Peron JP, Muotri AR, Beltrao-Braga PC. 2016. The
760 Brazilian Zika virus strain causes birth defects in experimental models. Nature
761 534:267-271.

762 5. Driggers RW, Ho CY, Korhonen EM, Kuivanen S, Jaaskelainen AJ, Smura T,
763 Rosenberg A, Hill DA, DeBiasi RL, Vezina G, Timofeev J, Rodriguez FJ, Levanov L,
764 Razak J, Iyengar P, Hennenfent A, Kennedy R, Lanciotti R, du Plessis A, Vapalahti
765 O. 2016. Zika Virus Infection with Prolonged Maternal Viremia and Fetal Brain
766 Abnormalities. N Engl J Med 374:2142-2151.

767 6. Garcez PP, Loiola EC, Madeiro da Costa R, Higa LM, Trindade P, Delvecchio R,
768 Nascimento JM, Brindeiro R, Tanuri A, Rehen SK. 2016. Zika virus impairs growth
769 in human neurospheres and brain organoids. Science 352:816-818.

770 7. Mlakar J, Korva M, Tul N, Popovic M, Poljsak-Prijatelj M, Mraz J, Kolenc M,
771 Resman Rus K, Vesnaver Vipotnik T, Fabjan Vodusek V, Vizjak A, Pizem J,
772 Petrovec M, Avsic Zupanc T. 2016. Zika Virus Associated with Microcephaly. N
773 Engl J Med 374:951-958.

774 8. Tang H, Hammack C, Ogden SC, Wen Z, Qian X, Li Y, Yao B, Shin J, Zhang F, Lee
775 EM, Christian KM, Didier RA, Jin P, Song H, Ming GL. 2016. Zika Virus Infects
776 Human Cortical Neural Progenitors and Attenuates Their Growth. Cell Stem Cell
777 doi:10.1016/j.stem.2016.02.016.

778 9. Halstead SB, Dans LF. 2019. Dengue infection and advances in dengue vaccines for
779 children. Lancet Child Adolesc Health 3:734-741.

780 10. Mercorelli B, Palu G, Loregian A. 2018. Drug Repurposing for Viral Infectious
781 Diseases: How Far Are We? Trends Microbiol doi:10.1016/j.tim.2018.04.004.

782 11. Barrows NJ, Campos RK, Powell ST, Prasanth KR, Schott-Lerner G, Soto-Acosta R,
783 Galarza-Munoz G, McGrath EL, Urrabaz-Garza R, Gao J, Wu P, Menon R, Saade G,
784 Fernandez-Salas I, Rossi SL, Vasilakis N, Routh A, Bradrick SS, Garcia-Blanco MA.
785 2016. A Screen of FDA-Approved Drugs for Inhibitors of Zika Virus Infection. Cell
786 Host Microbe 20:259-270.
787 12. Rausch K, Hackett BA, Weinbren NL, Reeder SM, Sadovsky Y, Hunter CA, Schultz
788 DC, Coyne CB, Cherry S. 2017. Screening Bioactives Reveals Nanchangmycin as a
789 Broad Spectrum Antiviral Active against Zika Virus. Cell Rep 18:804-815.
790 13. Xu M, Lee EM, Wen Z, Cheng Y, Huang WK, Qian X, Tcw J, Kouznetsova J, Ogden
791 SC, Hammack C, Jacob F, Nguyen HN, Itkin M, Hanna C, Shinn P, Allen C, Michael
792 SG, Simeonov A, Huang W, Christian KM, Goate A, Brennand KJ, Huang R, Xia M,
793 Ming GL, Zheng W, Song H, Tang H. 2016. Identification of small-molecule
794 inhibitors of Zika virus infection and induced neural cell death via a drug repurposing
795 screen. Nat Med 22:1101-1107.
796 14. Zhou T, Tan L, Cederquist GY, Fan Y, Hartley BJ, Mukherjee S, Tomishima M,
797 Brennand KJ, Zhang Q, Schwartz RE, Evans T, Studer L, Chen S. 2017. High-
798 Content Screening in hPSC-Neural Progenitors Identifies Drug Candidates that Inhibit
799 Zika Virus Infection in Fetal-like Organoids and Adult Brain. Cell Stem Cell 21:274-
800 283.e275.
801 15. Hanners NW, Eitson JL, Usui N, Richardson RB, Wexler EM, Konopka G, Schoggins
802 JW. 2016. Western Zika Virus in Human Fetal Neural Progenitors Persists Long Term
803 with Partial Cytopathic and Limited Immunogenic Effects. Cell Rep 15:2315-2322.
804 16. Richardson RB, Ohlson MB, Eitson JL, Kumar A, McDougal MB, Boys IN, Mar KB,
805 De La Cruz-Rivera PC, Douglas C, Konopka G, Xing C, Schoggins JW. 2018. A

806 CRISPR screen identifies IFI6 as an ER-resident interferon effector that blocks
807 flavivirus replication. Nat Microbiol 3:1214-1223.

808 17. Birmingham A, Selfors LM, Forster T, Wrobel D, Kennedy CJ, Shanks E, Santoyo-
809 Lopez J, Dunican DJ, Long A, Kelleher D, Smith Q, Beijersbergen RL, Ghazal P,
810 Shamu CE. 2009. Statistical methods for analysis of high-throughput RNA
811 interference screens. Nat Methods 6:569-575.

812 18. Chu JJ, Yang PL. 2007. c-Src protein kinase inhibitors block assembly and maturation
813 of dengue virus. Proc Natl Acad Sci U S A 104:3520-3525.

814 19. Miner JJ, Cao B, Govero J, Smith AM, Fernandez E, Cabrera OH, Garber C, Noll M,
815 Klein RS, Noguchi KK, Mysorekar IU, Diamond MS. 2016. Zika Virus Infection
816 during Pregnancy in Mice Causes Placental Damage and Fetal Demise. Cell
817 165:1081-1091.

818 20. Sheridan MA, Yunusov D, Balaraman V, Alexenko AP, Yabe S, Verjovski-Almeida
819 S, Schust DJ, Franz AW, Sadovsky Y, Ezashi T, Roberts RM. 2017. Vulnerability of
820 primitive human placental trophoblast to Zika virus. Proc Natl Acad Sci U S A
821 114:E1587-e1596.

822 21. Levenson AS, Jordan VC. 1997. MCF-7: the first hormone-responsive breast cancer
823 cell line. Cancer Res 57:3071-3078.

824 22. Andersson S, Sundberg M, Pristovsek N, Ibrahim A, Jonsson P, Katona B, Clausson
825 CM, Zieba A, Ramstrom M, Soderberg O, Williams C, Asplund A. 2017. Insufficient
826 antibody validation challenges oestrogen receptor beta research. Nat Commun
827 8:15840.

828 23. Nelson AW, Groen AJ, Miller JL, Warren AY, Holmes KA, Tarulli GA, Tilley WD,
829 Katzenellenbogen BS, Hawse JR, Gnanapragasam VJ, Carroll JS. 2017.
830 Comprehensive assessment of estrogen receptor beta antibodies in cancer cell line

models and tissue reveals critical limitations in reagent specificity. Mol Cell Endocrinol 440:138-150.

24. Eyre NS, Johnson SM, Eltahla AA, Aloi M, Aloia AL, McDevitt CA, Bull RA, Beard MR. 2017. Genome-Wide Mutagenesis of Dengue Virus Reveals Plasticity of the NS1 Protein and Enables Generation of Infectious Tagged Reporter Viruses. J Virol 91.

25. Mingorance L, Friesland M, Coto-Llerena M, Perez-del-Pulgar S, Boix L, Lopez-Oliva JM, Bruix J, Forns X, Gastaminza P. 2014. Selective inhibition of hepatitis C virus infection by hydroxyzine and benztropine. Antimicrob Agents Chemother 58:3451-3460.

26. Murakami Y, Fukasawa M, Kaneko Y, Suzuki T, Wakita T, Fukazawa H. 2013. Selective estrogen receptor modulators inhibit hepatitis C virus infection at multiple steps of the virus life cycle. Microbes Infect 15:45-55.

27. Watashi K, Inoue D, Hijikata M, Goto K, Aly HH, Shimotohno K. 2007. Anti-hepatitis C virus activity of tamoxifen reveals the functional association of estrogen receptor with viral RNA polymerase NS5B. J Biol Chem 282:32765-32772.

28. Dong S, Kang S, Dimopoulos G. 2019. Identification of anti-flaviviral drugs with mosquitocidal and anti-Zika virus activity in Aedes aegypti. PLoS Negl Trop Dis 13:e0007681.

29. Salata C, Calistri A, Parolin C, Baritussio A, Palu G. 2017. Antiviral activity of cationic amphiphilic drugs. Expert Rev Anti Infect Ther 15:483-492.

30. de Wilde AH, Jochmans D, Posthuma CC, Zevenhoven-Dobbe JC, van Nieuwkoop S, Bestebroer TM, van den Hoogen BG, Neyts J, Snijder EJ. 2014. Screening of an FDA-approved compound library identifies four small-molecule inhibitors of Middle

East respiratory syndrome coronavirus replication in cell culture. Antimicrob Agents Chemother 58:4875-4884.

31. Johansen LM, Brannan JM, Delos SE, Shoemaker CJ, Stossel A, Lear C, Hoffstrom BG, Dewald LE, Schornberg KL, Scully C, Lehar J, Hensley LE, White JM, Olinger GG. 2013. FDA-approved selective estrogen receptor modulators inhibit Ebola virus infection. Sci Transl Med 5:190ra179.

32. Johansen LM, DeWald LE, Shoemaker CJ, Hoffstrom BG, Lear-Rooney CM, Stossel A, Nelson E, Delos SE, Simmons JA, Grenier JM, Pierce LT, Pajouhesh H, Lehar J, Hensley LE, Glass PJ, White JM, Olinger GG. 2015. A screen of approved drugs and molecular probes identifies therapeutics with anti-Ebola virus activity. Sci Transl Med 7:290ra289.

33. Kouznetsova J, Sun W, Martinez-Romero C, Tawa G, Shinn P, Chen CZ, Schimmer A, Sanderson P, McKew JC, Zheng W, Garcia-Sastre A. 2014. Identification of 53 compounds that block Ebola virus-like particle entry via a repurposing screen of approved drugs. Emerg Microbes Infect 3:e84.

34. Madrid PB, Panchal RG, Warren TK, Shurtleff AC, Endsley AN, Green CE, Kolokoltsov A, Davey R, Manger ID, Gilfillan L, Bavari S, Tanga MJ. 2015. Evaluation of Ebola Virus Inhibitors for Drug Repurposing. ACS Infect Dis 1:317-326.

35. Zhao Y, Ren J, Harlos K, Jones DM, Zeltina A, Bowden TA, Padilla-Parra S, Fry EE, Stuart DI. 2016. Toremifene interacts with and destabilizes the Ebola virus glycoprotein. Nature 535:169-172.

36. Fan H, Du X, Zhang J, Zheng H, Lu X, Wu Q, Li H, Wang H, Shi Y, Gao G, Zhou Z, Tan DX, Li X. 2017. Selective inhibition of Ebola entry with selective estrogen receptor modulators by disrupting the endolysosomal calcium. Sci Rep 7:41226.

880 37. Lu F, Liang Q, Abi-Mosleh L, Das A, De Brabander JK, Goldstein JL, Brown MS.
881 2015. Identification of NPC1 as the target of U18666A, an inhibitor of lysosomal
882 cholesterol export and Ebola infection. Elife 4.
883 38. Poh MK, Shui G, Xie X, Shi PY, Wenk MR, Gu F. 2012. U18666A, an intra-cellular
884 cholesterol transport inhibitor, inhibits dengue virus entry and replication. Antiviral
885 Res 93:191-198.
886 39. Stoeck IK, Lee JY, Tabata K, Romero-Brey I, Paul D, Schult P, Lohmann V, Kaderali
887 L, Bartenschlager R. 2018. Hepatitis C Virus Replication Depends on Endosomal
888 Cholesterol Homeostasis. J Virol 92.
889 40. Fernandez-Suarez ME, Escola-Gil JC, Pastor O, Davalos A, Blanco-Vaca F,
890 Lasuncion MA, Martinez-Botas J, Gomez-Coronado D. 2016. Clinically used
891 selective estrogen receptor modulators affect different steps of macrophage-specific
892 reverse cholesterol transport. Sci Rep 6:32105.
893 41. Tohma D, Tajima S, Kato F, Sato H, Kakisaka M, Hishiki T, Kataoka M, Takeyama
894 H, Lim CK, Aida Y, Saijo M. 2019. An estrogen antagonist, cyclofenil, has anti-
895 dengue-virus activity. Arch Virol 164:225-234.
896 42. Neufeldt CJ, Cortese M, Acosta EG, Bartenschlager R. 2018. Rewiring cellular
897 networks by members of the Flaviviridae family. Nat Rev Microbiol 16:125-142.
898 43. Montoya MC, Krysan DJ. 2018. Repurposing Estrogen Receptor Antagonists for the
899 Treatment of Infectious Disease. mBio 9.
900 44. Blight KJ, McKeating JA, Rice CM. 2002. Highly permissive cell lines for
901 subgenomic and genomic hepatitis C virus RNA replication. J Virol 76:13001-13014.
902 45. Eyre NS, Hampton-Smith RJ, Aloia AL, Eddes JS, Simpson KJ, Hoffmann P, Beard
903 MR. 2016. Phosphorylation of NS5A Serine-235 is essential to hepatitis C virus RNA
904 replication and normal replication compartment formation. Virology 491:27-44.

905 46. Van der Hoek KH, Eyre NS, Shue B, Khantisitthiporn O, Glab-Ampi K, Carr JM,
906 Gartner MJ, Jolly LA, Thomas PQ, Adikusuma F, Jankovic-Karasoulos T, Roberts
907 CT, Helbig KJ, Beard MR. 2017. Viperin is an important host restriction factor in
908 control of Zika virus infection. Sci Rep 7:4475.
909 47. Eyre NS, Aloia AL, Joyce MA, Chulanetra M, Tyrrell DL, Beard MR. 2017. Sensitive
910 luminescent reporter viruses reveal appreciable release of hepatitis C virus NS5A
911 protein into the extracellular environment. Virology 507:20-31.
912 48. Fischl W, Bartenschlager R. 2013. High-throughput screening using dengue virus
913 reporter genomes. Methods Mol Biol 1030:205-219.
914 49. Munster M, Plaszczyca A, Cortese M, Neufeldt CJ, Goellner S, Long G,
915 Bartenschlager R. 2018. A Reverse Genetics System for Zika Virus Based on a
916 Simple Molecular Cloning Strategy. Viruses 10.
917 50. Eltahla AA, Lackovic K, Marquis C, Eden JS, White PA. 2013. A fluorescence-based
918 high-throughput screen to identify small compound inhibitors of the genotype 3a
919 hepatitis C virus RNA polymerase. J Biomol Screen 18:1027-1034.
920 51. Eltahla AA, Tay E, Douglas MW, White PA. 2014. Cross-genotypic examination of
921 hepatitis C virus polymerase inhibitors reveals a novel mechanism of action for thumb
922 binders. Antimicrob Agents Chemother 58:7215-7224.
923 52. Eyre NS, Drummer HE, Beard MR. 2010. The SR-BI partner PDZK1 facilitates
924 hepatitis C virus entry. PLoS Pathog 6:e1001130.

925

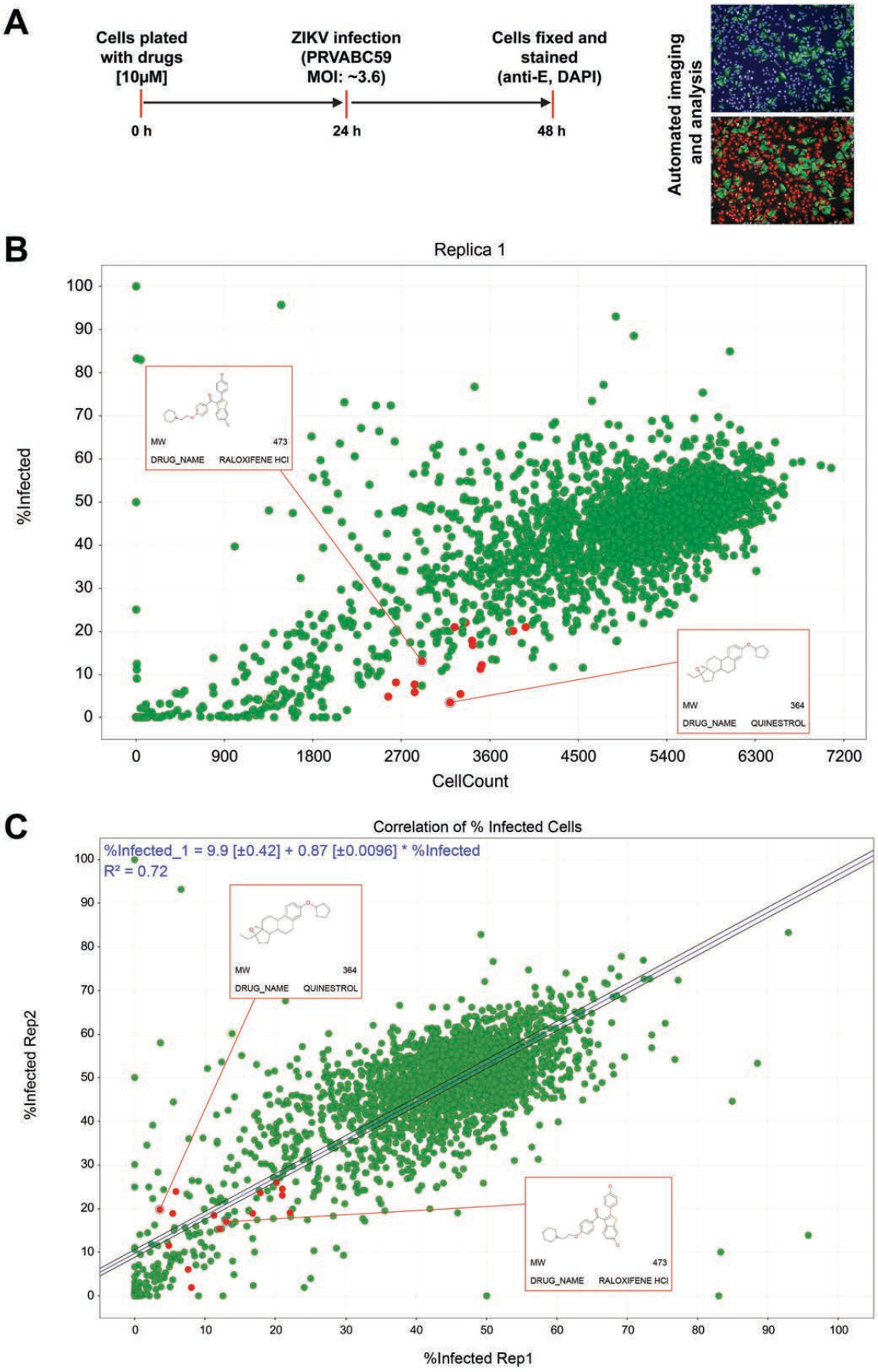

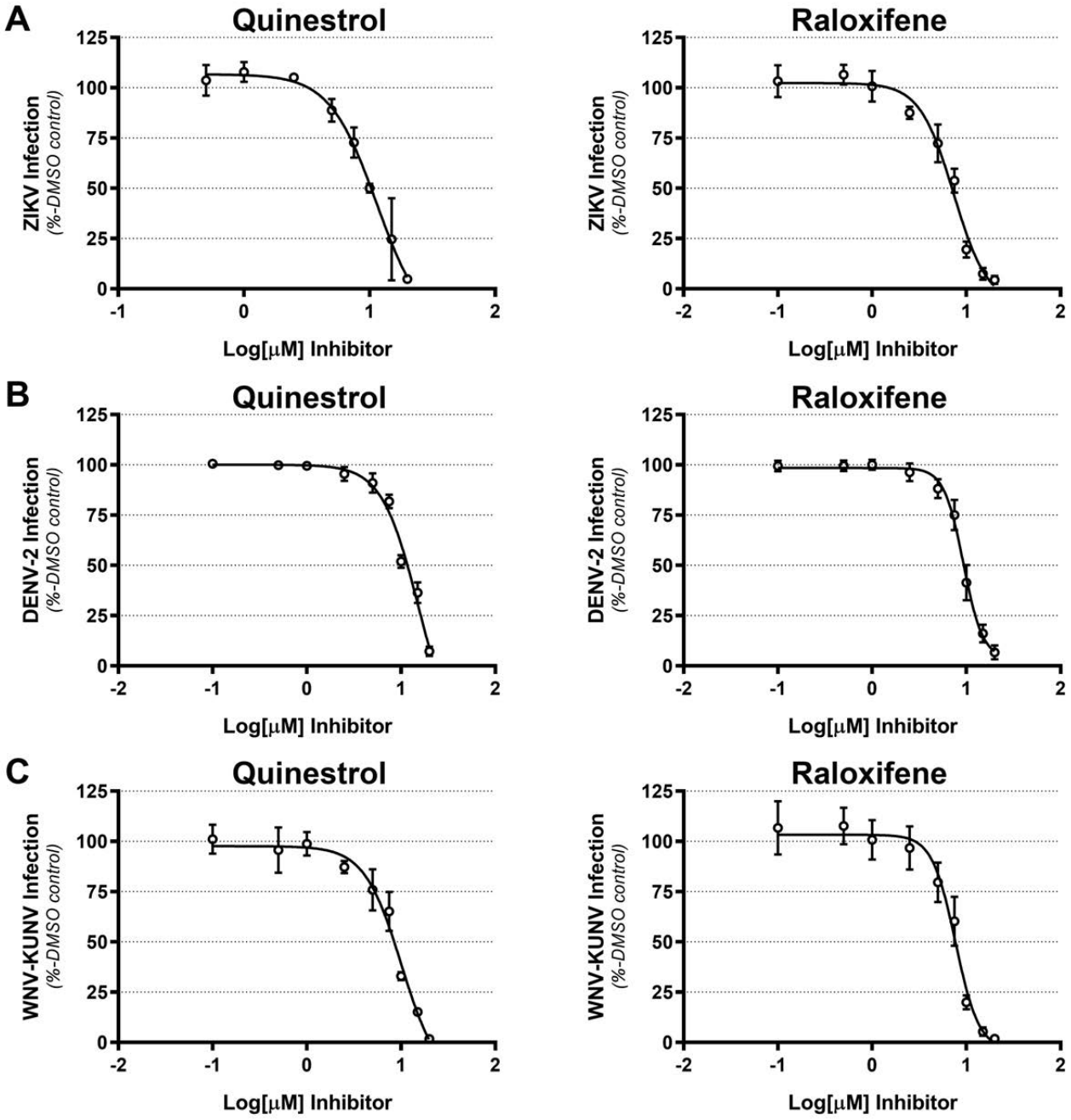

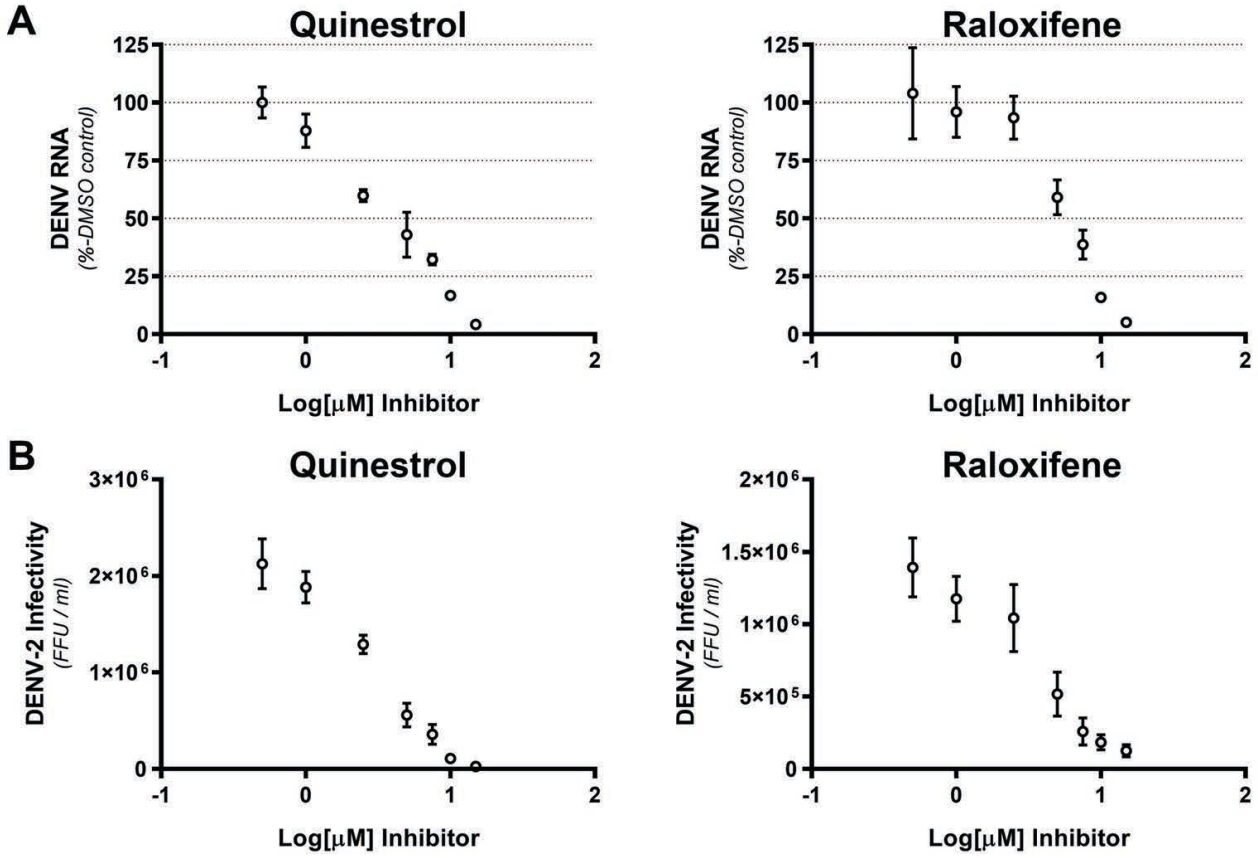

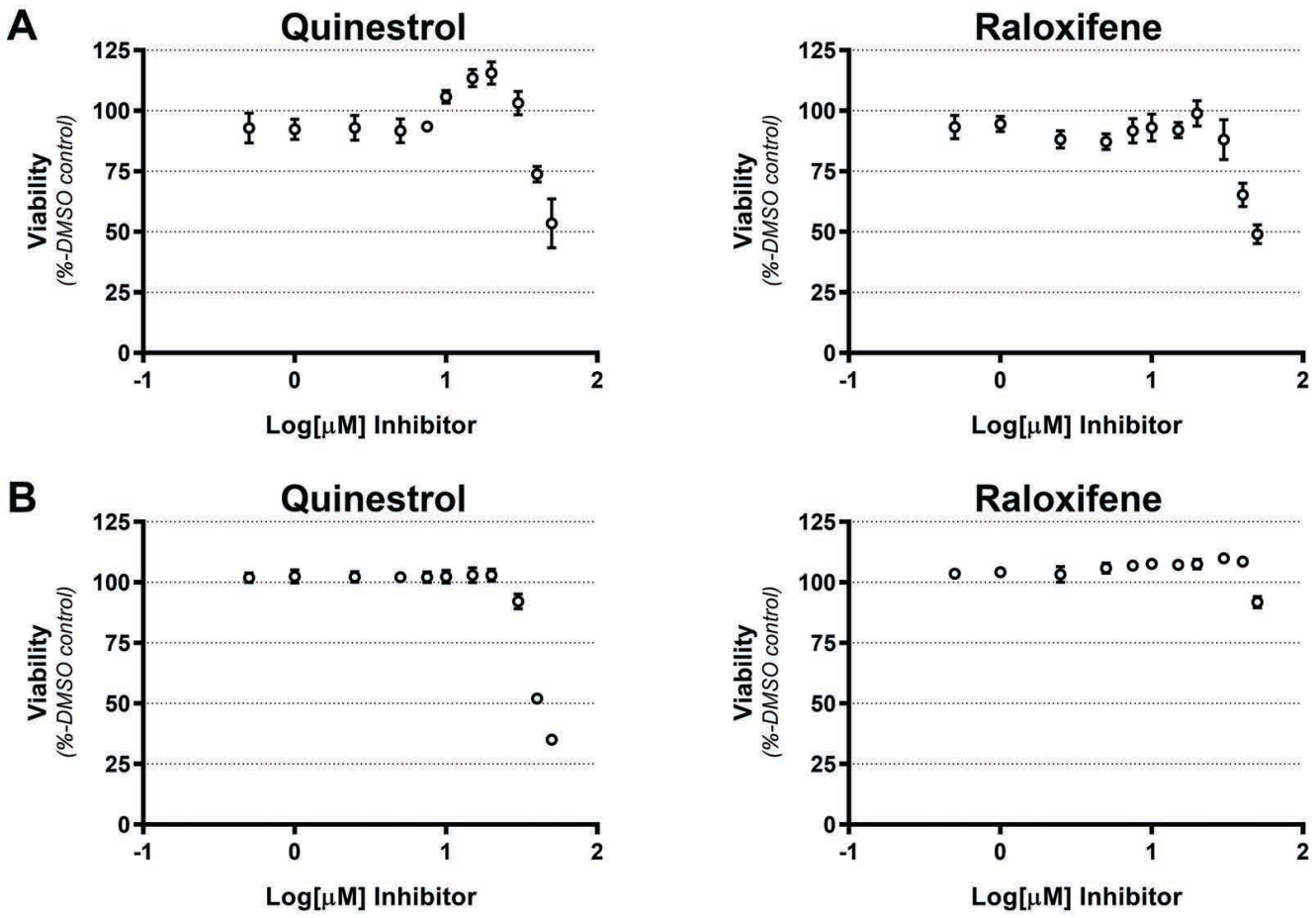

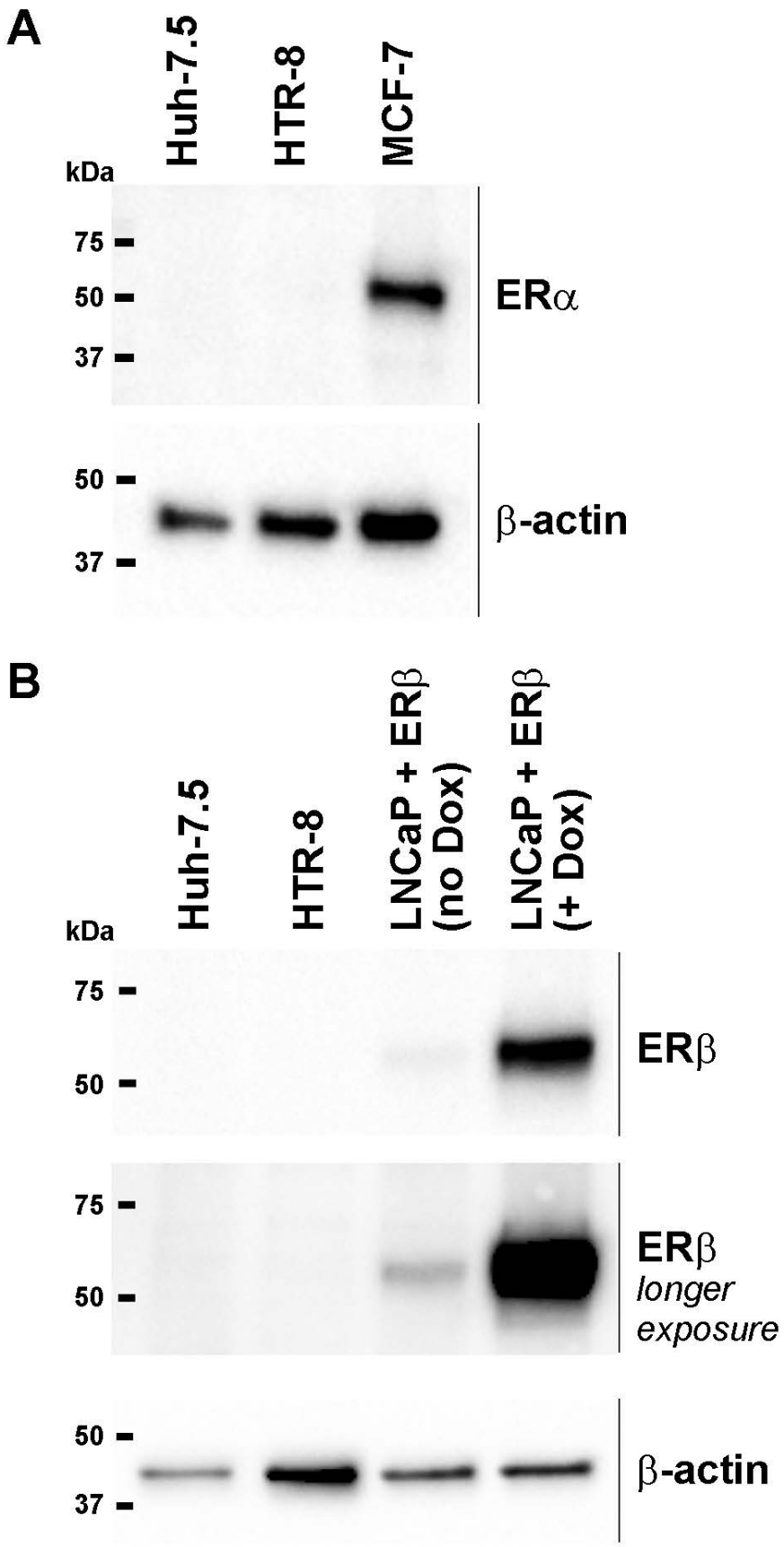

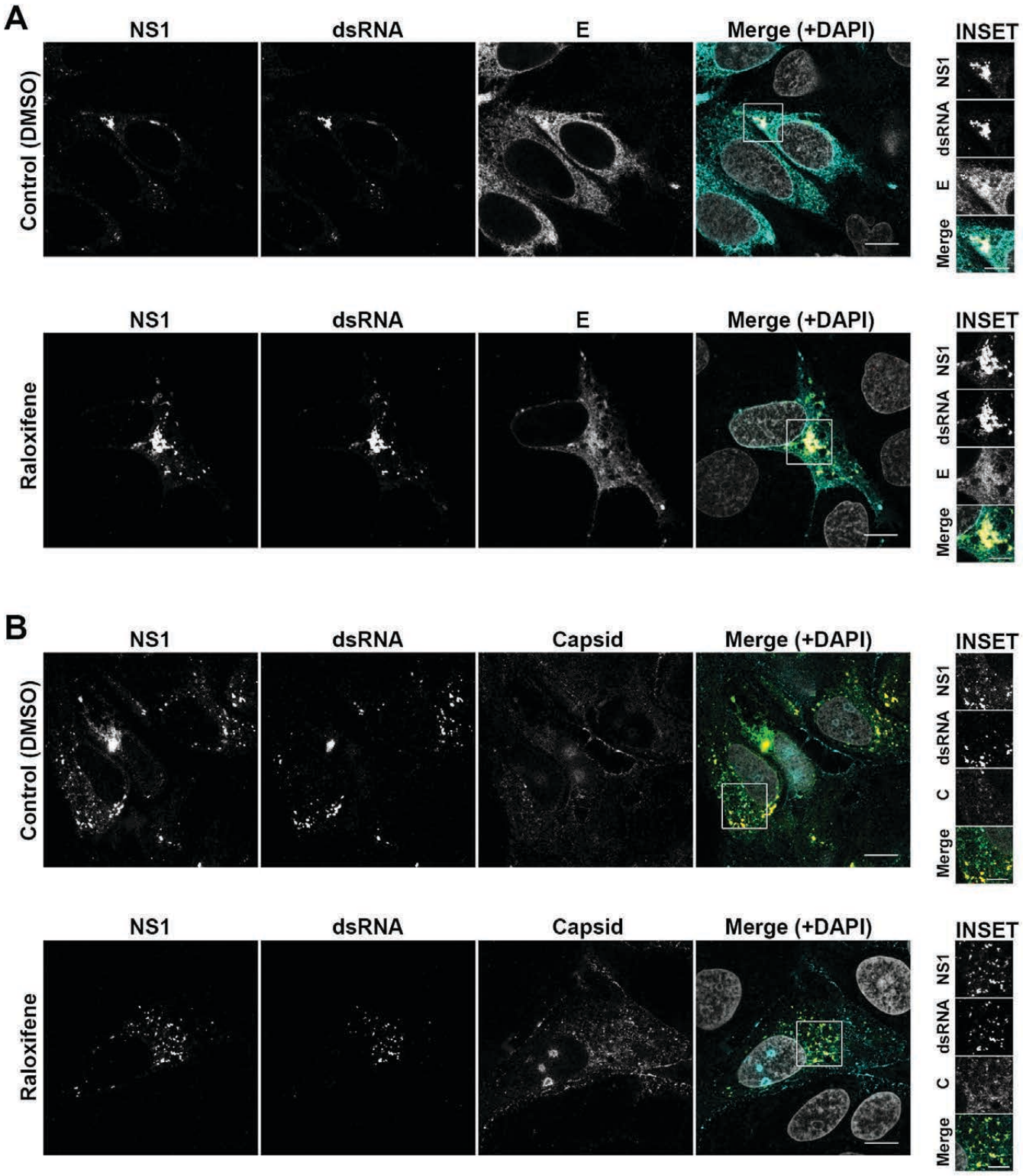

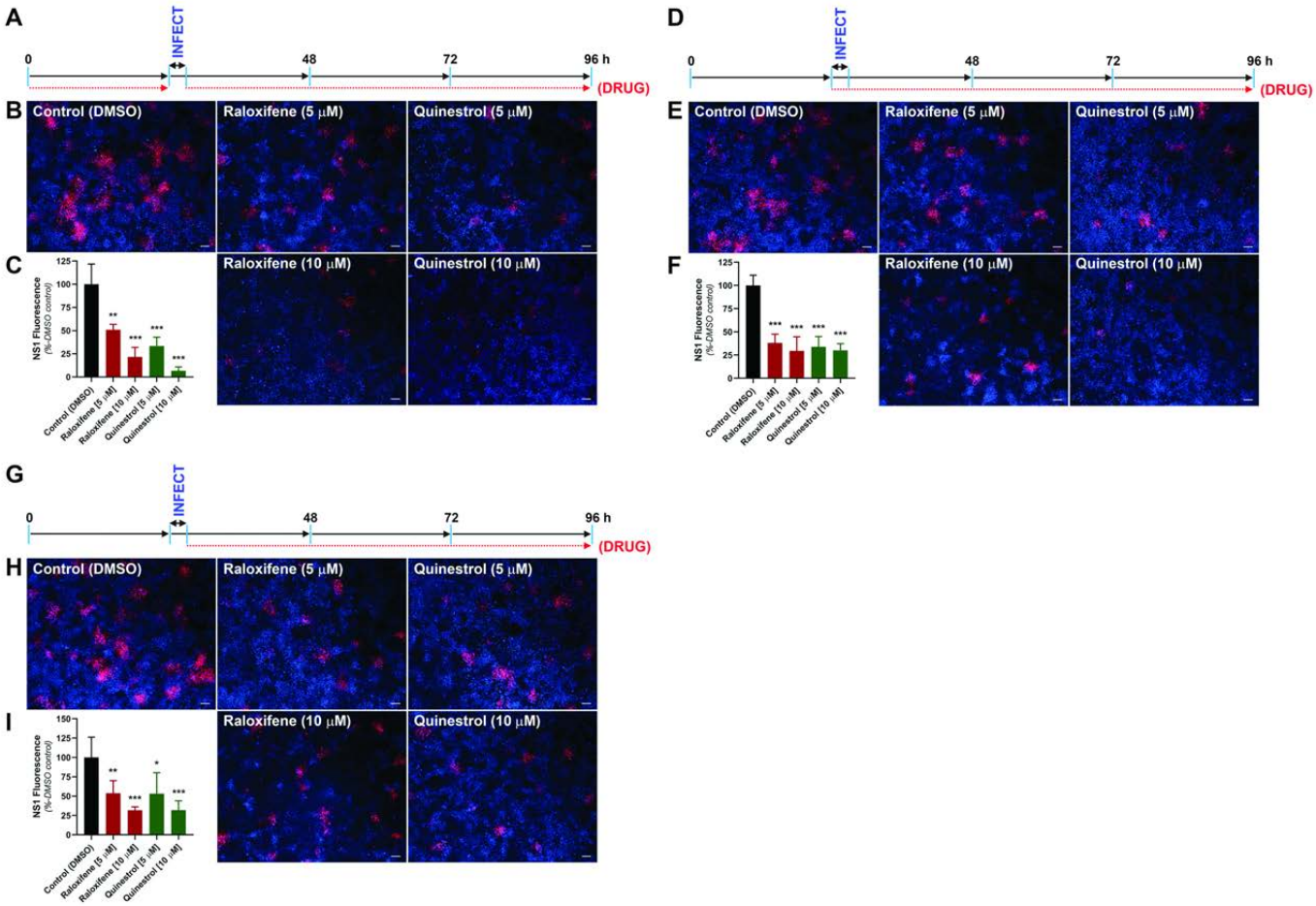

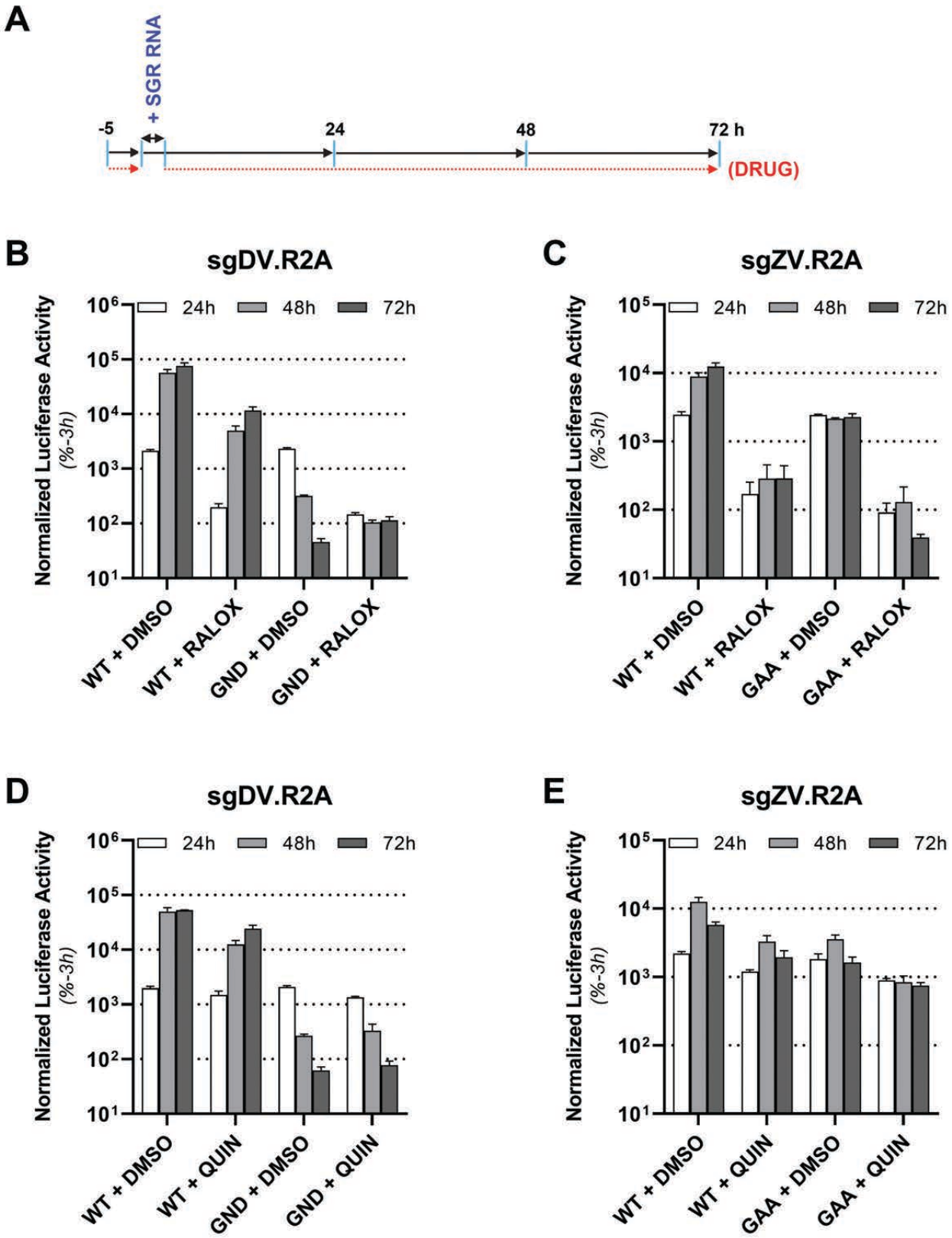

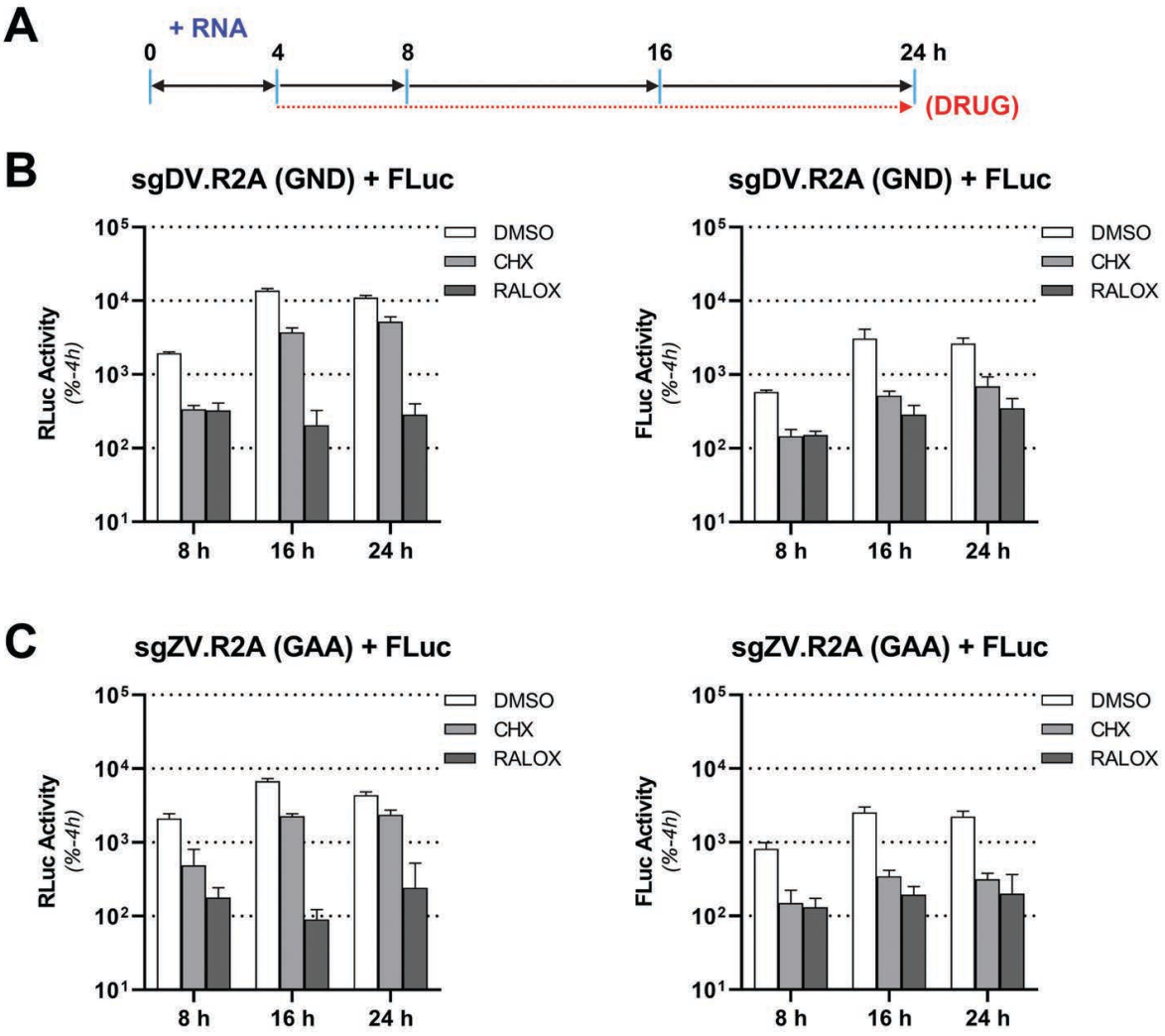

Drug Name	Robust Z-score (Rep 1)	Robust Z-score (Rep 2)	%-Infected (Rep 1)	%-Infected (Rep 2)
QUINESTROL	-8.960543891	-10.40147721	3.54	19.83
RALOXIFENE	-5.594885708	-6.664829682	13.02	16.98
CITRININ	-6.458823564	-8.277304205	22.06	19.13
CHLORHEXIDINE DIHYDROCHLORIDE	-9.529448426	-13.20775169	8.09	11.57
TIOGUANINE	-12.91379595	-11.24947726	4.83	11.57
CHLORINDANOL	-5.29865036	-6.151139657	16.77	18.86
ERYTHRITOL	-6.462380225	-7.869080309	20.95	23.09
IMATINIB BASE	-4.07701258	-5.876354389	20.94	24.46
ENROFLOXACIN	-4.10359615	-4.224948397	5.42	18.89
DEOXYSAPPANONE B TRIMETHYL ETHER	-4.028366822	-3.388602238	5.82	23.99
AZELASTINE HYDROCHLORIDE	-9.859143907	-8.477809972	17.89	23.69
ARTENIMOL	-7.181930945	-3.669083741	12.12	15.32
DEQUALINIUM CHLORIDE	-7.542871498	-10.03461574	7.62	6.02
DEACETYLGEDUNIN	-6.798053157	-7.180822605	11.24	18.48
ARTESUNATE	-4.975058417	-5.45911868	20.1	26

Table 1. Inhibitors of ZIKV infection in Huh-7.5 cells identified via high-throughput screening.